REPORT DOCUMENTATION PAGE Dist: A

Form Approved
OMB No. 0704-0188

1. AGENCY USE ONLY (Leave blank)	2. REPORT DATE	3. REPORT TYPE AND DATES COVERED
	March 1994	Final Tech. Rep. 2/15/91 - 2/14/94

4. TITLE AND SUBTITLE

(U) Transport Phenomena and Interfacial Kinetics in Multiphase Combustion Systems

5. FUNDING NUMBERS

PE - 61102F
PR - 2308
SA - BS
G - AFOSR 91-0170

6. AUTHOR(S)

Principal Investigator: Daniel E. Rosner

7. PERFORMING ORGANIZATION NAME(S) AND ADDRESS(ES)

HIGH TEMPERATURE CHEMICAL REACTION ENGINEERING LABORATORY
YALE UNIVERSITY
BOX 208286 YALE STATION
NEW HAVEN, CONNECTICUT 06520 U.S.A.

8. PERFORMING ORGANIZATION REPORT NUMBER

AFOSR-TR- 94 0691

9. SPONSORING/MONITORING AGENCY NAME(S) AND ADDRESS(ES)

AFOSR/NA
110 Duncan Avenue, Suite B115
Bolling AFB DC 20332-0001

10. SPONSORING/MONITORING AGENCY REPORT NUMBER

11. SUPPLEMENTARY NOTES

12a. DISTRIBUTION/AVAILABILITY STATEMENT

Approved for public release; distribution is unlimited

A

12b. DISTRIBUTION CODE

13. ABSTRACT (Maximum 200 words)

This *final technical report* summarizes Yale High Temperature Chemical Reaction Engineering Laboratory research activities (under Grant AFOSR 91-0170) for the three-year period ending 14 February 1994. Among our research *results* described in detail in the cited references (Section 5), perhaps the most noteworthy are the development/reporting of:

R1 rational methods to predict the *accessible surface area* and *translational Brownian diffusivity* of aggregated 'soot' particles in high pressure combustion gases

R2 experimental inference of particle *thermophoretic diffusivities* for titania aggregates in laminar counterflow laminar diffusion flames; consequences of particle thermophoresis for flame radiation, flame synthesis, and 'non-biased' thermophoretic sampling

R3 quantitative methods for predicting/correlating the effects vapor phase chemical reactions on the rate and quality of vapor-deposited ceramic thin films

Thirty verbal presentations, ten archival publications, and three PhDs have resulted from this research program. Additionally, nine papers are submitted or in press. Copies of the principal reprints appearing during the final year of this program are included in the Appendices (Section 6) of this report.

14. SUBJECT TERMS

Key Words: Soot, aggregated particles, mass transport, thermophoresis, particle inertia Brownian diffusion, chemical vapor deposition, particle sampling, deposit microstructure/properties

15. NUMBER OF PAGES 44

16. PRICE CODE

17. SECURITY CLASSIFICATION OF REPORT	18. SECURITY CLASSIFICATION OF THIS PAGE	19. SECURITY CLASSIFICATION OF ABSTRACT	20. LIMITATION OF ABSTRACT
Unclassified	Unclassified	Unclassified	UL

TRANSPORT PHENOMENA AND INTERFACIAL KINETICS IN MULTIPHASE COMBUSTION SYSTEMS

Principal Investigator: Prof. **Daniel E. Rosner**

1. INTRODUCTION

The performance of ramjets burning slurry fuels (leading to condensed oxide aerosols and liquid film deposits), gas turbine engines in dusty or marine atmospheres, or when using fuels from non-traditional sources, depends upon the formation and transport of small particles across non-isothermal combustion gas boundary layers (BLs). Even airbreathing engines burning "clean" hydrocarbon fuels can experience *soot* formation/deposition problems (*e.g.*, combustor liner burnout, accelerated turbine blade erosion and "hot" corrosion). Moreover, particle formation and transport are important in many chemical reactors used to synthesize or process aerospace materials (turbine blade coatings, optical waveguides, ceramic precursor powders, fibers for composites,...). Accordingly, our research is directed toward providing chemical propulsion systems engineers and materials-oriented engineers with new techniques and quantitative information on important particle- and vapor-mass transport mechanisms and rates.

The purpose of this report is to summarize our research methods and accomplishments under AFOSR Grant 91-0170 (Technical Monitor: J.M. Tishkoff) during the 3-year period: 15 February '91-14 February '94. Readers interested in greater detail than contained in Section 2 are advised to consult the published papers explicitly cited in Sections 2 and 5. Copies of any of these published papers (Section 5.2 and Appendix) or preprints (Section 5.3) can be obtained by writing to the PI: Prof. Daniel E. Rosner, at the Department of Chemical Engineering, Yale University, New Haven ,CT 06520-8286 USA. Comments on, or examples of, the *applications* of our research (Section 3.4) will be especially welcome.

An interactive experimental/theoretical approach has been used to gain understanding of performance-limiting chemical-, and mass/energy transfer-phenomena at or near interfaces. This included the development and exploitation of seeded laboratory burners (Section 2.1), new optical diagnostic techniques (Section 2.2) and flow reactors (Section 2.4). Resulting experimental rate data , together with the predictions of asymptotic theories (Section 2), were used as the basis for proposing and verifying simple viewpoints and effective engineering correlations wirth a rational basis for future design/optimization studies.

2. RESEARCH ACCOMPLISHMENTS

Most of the results we have obtained under Grant AFOSR 91-0170 during '91-'94 can be divided into the subsections below:

2.1. TRANSPORT AND STABILITY OF AGGREGATED PARTICLES: THEORY

The ability to reliably predict the transport properties and stability of *aggregated* flame-generated *particles* (carbonaceous soot, Al_2O_3, SiO_2,...) is important to many technologies, including chemical propulsion and refractory materials fabrication. The existence and character of such particles is also known to influence the "signature" of chemical propulsion devices.

The *Brownian diffusion-*, inertial-, and optical-properties of *aggregated* particles, as formed in sooting diffusion flames, are quite *sensitive* to size (*e.g.* number N of "primary" particles; see Fig. 1) and morphology (geometrical arrangement of the primary particles). In this program we developed methods to anticipate coagulation and deposition rates of suspended populations of such particles in combustion systems. As one example, we have recently developed improved and efficient methods for predicting the Stokes drag of large 'fractal' aggregates *via* a spatially variable porous sphere model (Tandon and Rosner,1994; Figs. 1, 2). Using the Stokes-Einstein equation, the results of Fig. 2 have been used to predict the Brownian diffusivity of such aggregates in the high pressure (near continuum-) limit (proportional to the product of the reciprocal of the ordinate of Fig. 2 and N^{-1/D_f}). This approach can be extended to predict the *thermophoretic diffusivity* of such aggregates, an important quantity we have recently found to be much less sensitive to size and morphology than the translational Brownian diffusivity (Rosner *et.al.* 1992). Indeed, this provides the theoretical basis for the *thermophoretic sampling* technique being employed in our current experimental studies (Section 2.2). These new methods/results, together with recent results on the *spread* of aggregate sizes in coagulating populations, can be used to predict wall *capture rates* by the mechanisms of convective-diffusion, turbulent eddy-impaction, and thermophoresis. Also developed in this program were efficient pseudo-continuum methods to predict chemical interactions between aggregates and their surrounding *vapor* environment---interactions which can lead to primary particle growth, or burn-out. In particular, we developed new and efficient methods to predict the "accessible surface area" of aggregates (expressed as a fraction , η, of the true surface area in Fig. 3), including its dependence on size (N), structure (fractal dimension, D_f), probing molecule reaction probability α, and pressure level (*via* Knudsen number based on primary particle diameter)(Rosner and Tandon, 1994).

Initiated in this program were studies of the *restructuring kinetics* of aggregates — *ie.* those factors which determine the observed size of the apparent "primary particles" comprising soot particles, and the "collapse" of surface area observed in some high temperature systems (Cohen and Rosner,1993). Toward this end, we developed new methods to characterize the morphology of multi-particle aggregates (Fig. 5) thermophoretically extracted from laminar CDFs in a new "slot" type burner (Fig. 4). One such "fingerprint" is the *pdf* of angles formed by triplets of primary particles (Fig. 6).

2.2. FORMATION, TRANSPORT AND STABILITY OF COMBUSTION-GENERATED PARTICLES: LAMINAR COUNTERFLOW DIFFUSION FLAME EXPERIMENTS

We have inferred the *thermophoretic diffusivity* of flame-generated submicron "soot" particles using two-phase flame structure measurements on ($TiCl_4$(g)-)seeded low strain-rate counterflow laminar diffusion flames (CDF-) (Gomez and Rosner, 1993). A knowledge of the relative positions of the gas and particle stagnation planes and the associated thermal and chemical environments can be used to control the composition and morphology of flame-synthesized particles. These factors should also influence particle production and *radiation* from *turbulent* non-premixed "sooting" flames, as discussed further in Gomez and Rosner, 1993.

To obtain fundamental information on nucleation, growth and aggregate restructuring, we developed an improved "slot-type" burner (Fig. 4) and introduced instruments to carry out *in situ* measurements of particle Brownian motion (*via* "dynamic light scattering"). We also developed a thermophoretic sampler to extract aggregates from various positions in the seeded-CDF for morphological analysis using transmission electron microscope (TEM) images (Fig. 5). Aggregate data obtained from CH_4 flames seeded with titanium tetra-isopropoxide (TTIP-) vapor are being being analyzed using new theoretical methods briefly outlined in Sections 2.1, 2.3.

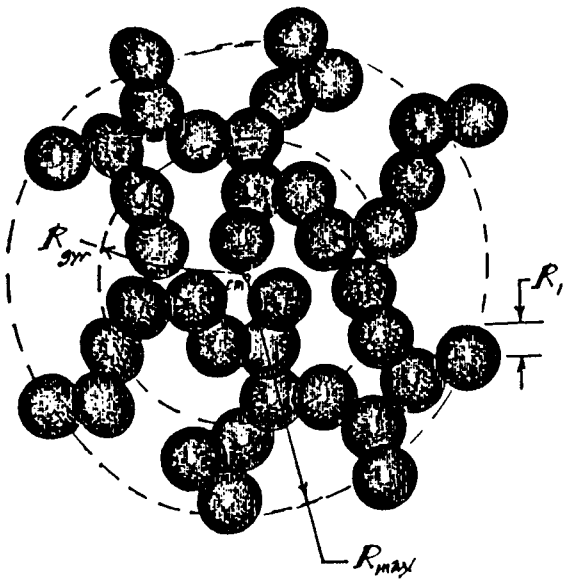

Fig.1 "Porous sphere" model of large fractal aggregate suspended in a background gas; basis for the calculation of translational and rotational Brownian diffusion coefficients, thermophoretic diffusivity, "stopping time", accessible area, and restructuring kinetics (after Rosner and Tandon, 1993, Rosner, Cohen and Tandon, 1993, Tandon and Rosner,1994)

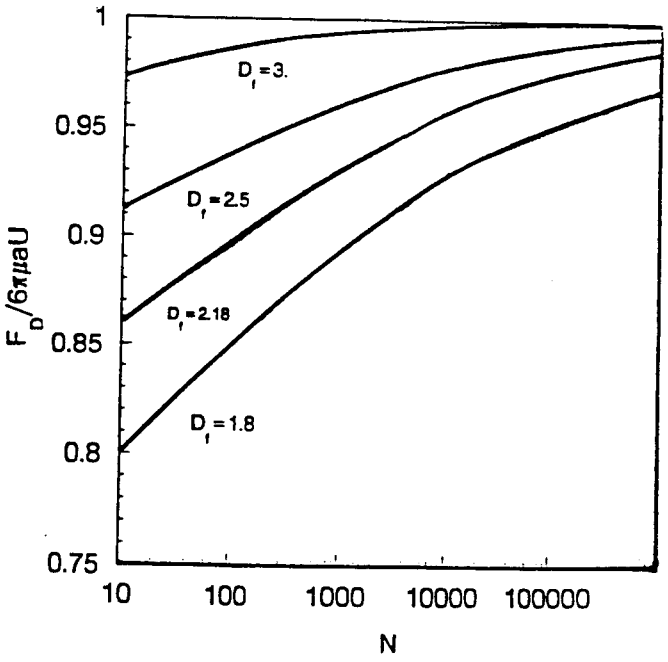

Fig. 2 Drag reduction associated with effective permeability for a quasi-spherical "fractal" aggregate comprised of N primary spheres in the continuum regime ($a = R_{max} = \{(3/2) \cdot [D_f+2)/D_f]\}^{1/2} R_{gyration}$) (after Tandon and Rosner, 1994)

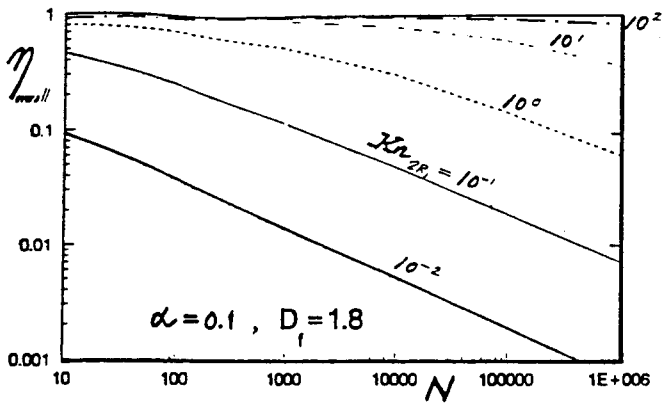

Fig. 3 Pressure dependence (*via* the Knudsen number based on primary sphere diameter) of the *accessible surface area* of large "open" (D_f=1.8) aggregates; reaction probability, α, of probing molecule 0.1; (after Rosner and Tandon, 1994)

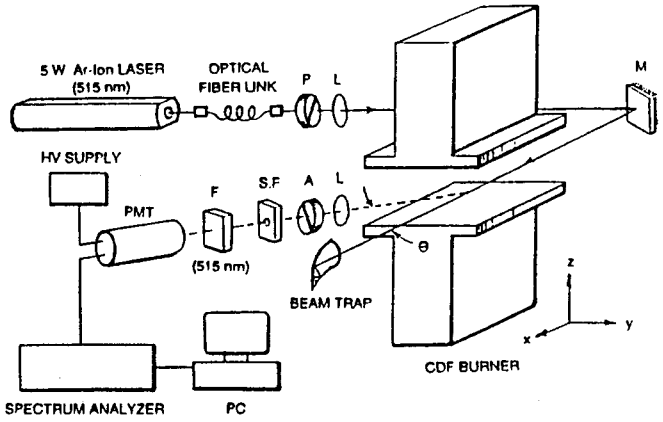

Fig.4 "Slot"-type counterflow diffusion flame (CDF-) burner set-up for *in situ* and extractive experimental studies of the nucleation, growth, transport and restructuring of aggregates in flames (after Albagli, Xing and Rosner, 1994; see, also Gomez and Rosner, 1993)

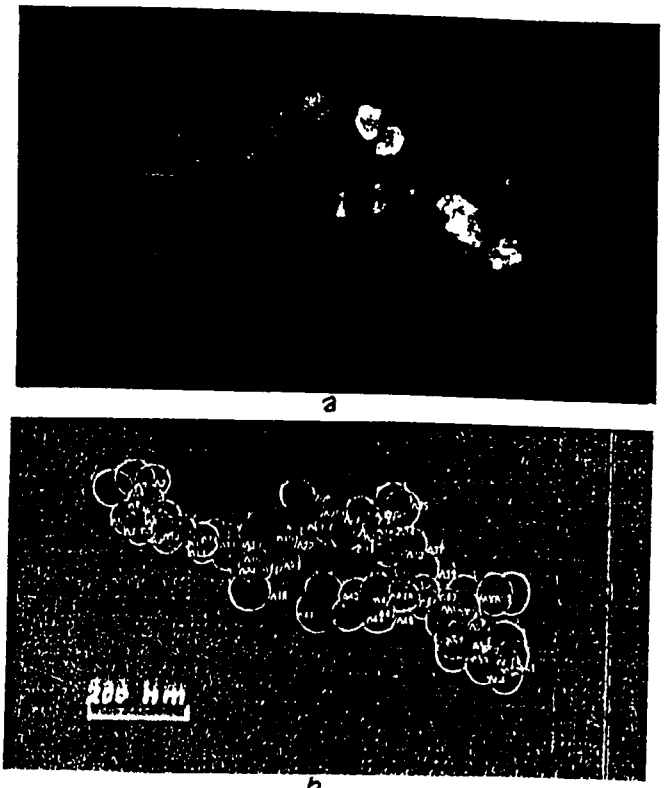

Fig. 5 Typical multiparticle aggregate thermophoretically extracted from laminar CDF seeded with TiO_2 precursor TTIP vapor. TEM image (a) compared to 'touching sphere' idealization (b) (after Albagli, Xing and Rosner,1994)

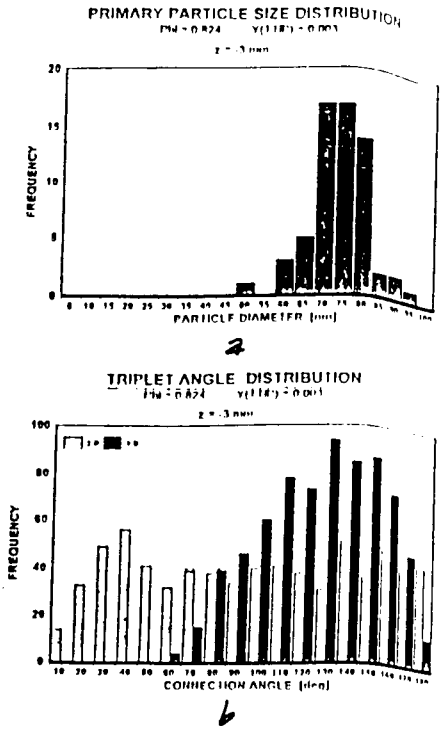

Fig. 6 Aggregate characterization techniques; (a) *pdf* of pimary particle diameters; (b) *pdf* of angles formed between triplets of contacting primary particles (2D: based on projected TEM image, 3D: corrected for three dimensionality of real aggregate] needed for restructuring kinetics analysis
(Cohen and Rosner, 1993,1994)

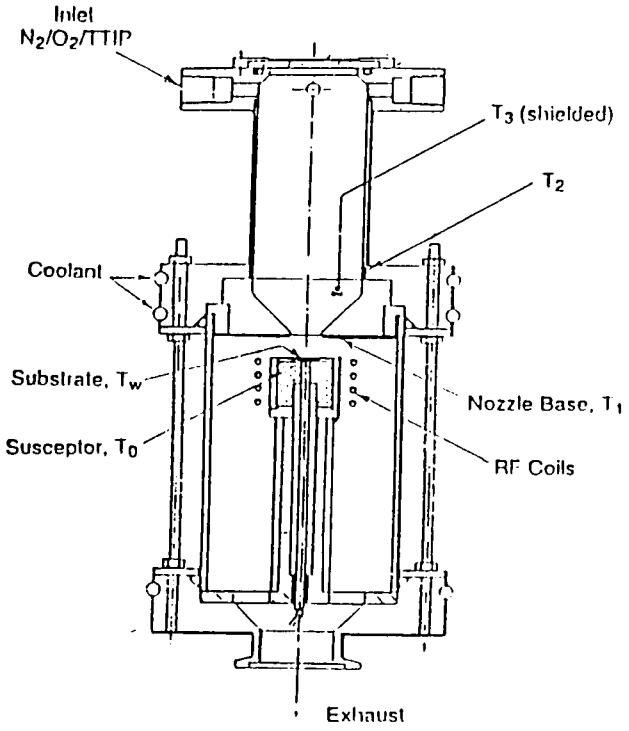

Fig. 7 Axisymmetric impinging jet CVD-reactor with inductively heated "pedestal" (after Rosner, Collins and Castillo, 1993, Collins,1994) for systematic studies of oxide film deposition from the vapor precursor TTIP

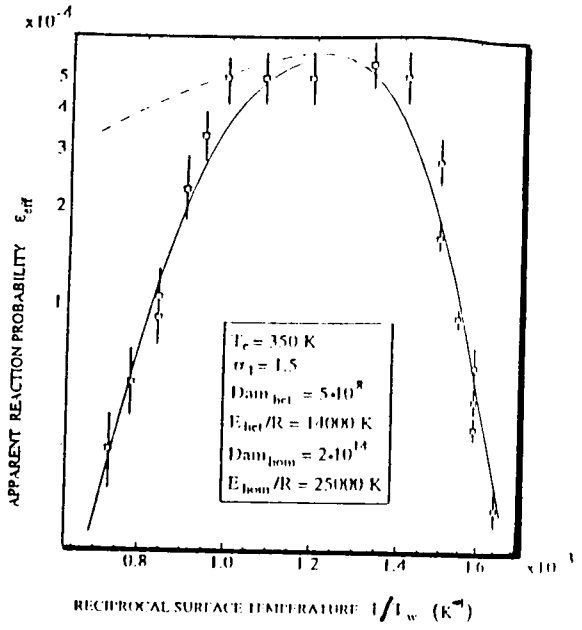

Fig.8 TiO_2(s) deposition rate data (reported as an apparent first order heterogeneous rate constant) from TTIP/O_2/N_2 mainstream showing 'best-fit' deposition rates (after Rosner, Collins and Castillo, 1993, Castillo and Rosner,1994) predicted using chemical sublayer (CSL-) theory, allowing for *homogeneous* consumption of TTIP within thermal BL.

2.3. MULTIPHASE TRANSPORT THEORY: NUCLEATION, GROWTH, THERMOPHORESIS AND INERTIA; AEROSOL SAMPLING IMPLICATIONS

In this program we have completed and submitted for *IJHMT* publication a comprehensive set of seeded micro-combustor experiments, and ancillary theoretical calculations on the interesting competition between particle *inertia* and particle *thermophoresis* for the case of particle transport across laminar nonisothermal gaseous boundary layers on surfaces with streamwise curvature (*e.g.*, turbine blades). (Konstandopoulos and Rosner, 1994). For *inertial impaction* we demonstrated that our earlier idea of correlating impingement rates from compressible gas flows using an *effective Stokes number* (Israel and Rosner, 1983) can be generalized to include the effects of aerodynamically interacting targets, as in a 'cascade' of turbine blades (Konstandopoulos, Labowsky and Rosner, 1993).

We also completed and published a computational study of the *unusual population dynamics* of coagulating absorbing-emitting particles in strong *radiation fields* (Mackowski *et.al.*, 1994). (For a useful overview of our recent AFOSR-supported work on these and other effects of energy transfer on suspended particle dynamics, see Rosner, *et. al.*, 1992).

The systematic effects of particle size/morphology-dependent wall deposition and coagulation on the sampling of aerosols have been predicted and discussed in 2 papers, one (Rosner and Tassopoulos, 1992) which appeared during this period, and one now in preparation (Rosner, Tandon and Konstandopoulos, 1994).

2.4. KINETICS AND MORPHOLOGY OF CVD-MATERIALS IN MULTI-PHASE ENVIRONMENTS

A small impinging jet (stagnation flow) reactor (Fig.7) has been developed and used to study the chemical vapor deposition (CVD-)-rates of refractory layers on inductively (over-)heated substrates (Collins, Rosner and Castillo,1992,1993; Collins, 1994). These measurements, initiated with the co-sponsorship of NASA-Lewis Labs, have been used to understand deposition rates and associated deposit microstructures observed in highly non-isothermal, often particle-containing local CVD environments. Figure 8 shows (logarithmic ordinate) our apparent deposition rate probabilities *vs.* reciprocal surface temperature for TiO_2(s) obtained from TTIP(g). The solid curve marked $Dam_{hom}= 2x\ 10^{14}$ (where this parameter may be regarded as a dimensionless homogeneous rate constant) shows our predicted CVD rate behavior including non-negligible Soret transport (Castillo and Rosner,1993) allowing for TTIP decomposition *within* the boundary layer. Agreement with the experimental data of Collins (1994) is encouraging indeed. Regarding deposit surface morphoplogy , we completed a theoretical study of the morphological stability of deposits growing by the mechanism of thermophoresis (or Soret transport for vapors) (chemical sublayer (CSL-) theory of Castillo, Garcia-Ybarra and Rosner, 1992). On the subject of the 'grain' density of vapor deposits we proposed and successfully demonstrated a rational correlation which relates the density of 7 materials (including SiC, BN and graphite) for which data could be found in the literature to their fundamental properties (activation energy for surface diffusion, lattice dimensions,...) and deposition conditions (reactant pressure, surface temperature, reaction probability) *via* a suitable Damkohler number which we call the 'burial' parameter (Kho, Collins and Rosner,1994).

In this program we have also summarized our research on the high temperature gasification kinetics of solid boron by B_2O_3(g), including the implications of our flow reactor data for chemical propulsion applications (Gomez, Rosner, and Zvuloni, 1993).

****

In our OSR-sponsored Yale HTCRE Lab research during this program, briefly reviewed here, we have shown that new methods for rapidly measuring particle transport rates, combined with recent advances in boundary layer theory, provide useful means to

identify and incorporate important, but often previously neglected, mass transport phenomena in many multiphase propulsion engineering and materials engineering design/optimization calculations.

Despite the formidable complexities to be overcome in the design and operation of air-breathing propulsion power plants utilizing a broad spectrum energetic fuels these particular techniques and results are indicative of the potentially useful simplifications and generalizations which have emerged from this program's fundamental AFOSR-funded research studies of combustion-generated particle transport mechanisms. It is hoped that this Final Report and its supporting (cited) papers will facilitate the refinement and/or incorporation of some of the present ideas into engineering design procedures of much greater generality and reliability. This work has already helped identify new directions where research results could have a significant impact on engineering practice in both the defense and civilian sectors of the US economy (Section 3.4).

3. ADMINISTRATIVE INFORMATION: PERSONNEL, PRESENTATIONS, APPLICATIONS, "COUPLING' ACTIVITIES

The following sections summarize some pertinent 'non-technical' facets of the abovementioned Yale HTCRE Lab/AFOSR research program:

3.1 Personnel

The present results (Sections 2 and 5) are due to the contributions of the individuals listed in Table 3.1-1, which also indicates the role of each researcher and the relevant time interval of the activity. It will be noted that, in addition to the results themselves, this program has simultaneously contributed to the research training of a number of students and 3 recent PhDs, who will now be in an excellent position to make future contributions to technologies oriented toward air-breathing chemical propulsion, and high-tech materials processing.

Table 3.1-1 Summary of *Research Participants*[a] on AFOSR Grant :

TRANSPORT PHENOMENA AND INTERFACIAL KINETICS IN MULTIPHASE COMBUSTION SYSTEMS

Name	Status[a]	Date(s)	Principal Research Activity[b]
Albagli, D.	PDRA	4/92-5/94	particle prod/char. in CDFs
Cohen, R. D.	VS	Spring'93	aggregate restructuring theory
Collins, J.	GRA	'92-'94	CVD of ceramic coatings
Gomez, A.	Asst.Prof.	'92	Ms. on particle transp. props.(CDFs)
Kho,T.	GRA	'92-'94	correl. of density of CVD coatings
Konstandopoulos, A	GRA,PDRA	'92, '93	combined inertia + thermophoresis
Labowsky, M. J.	VS	'91-'94	inertial impaction and erosion
Papadopoulos, D	GRA	'92-'94	boundary conditions at G/S interface
Rosner, D.E.	PI	'91-'94	program direction-dep. theory/exp
Silverman, I.	PDRA	'92-'93	spray evap/comb. at high pressures
Tandon, P.	GRA	'92-'94	transport phenom. in BLs and CDFs
Xing, Y.	GRA	'93-'94	particle prod/char. in CDFs

[a] PDRA=Post-doctoral Research Asst GRA= Graduate Research Assistant
PI = Principal Investigator VS = Visiting Scholar

[b] See Section 5 for specific references cited in text (Section 2)

3.2 Cooperation with US Industry

The research summarized here was supported by AFOSR under Grant 91-0170 (2/15/91-2/14/94). The Yale HTCRE Laboratory has also been the beneficiary of continuing smaller grants from U.S. industrial corporations, including groups within GE, DuPont, Union Carbide (now Advanced Ceramics Corp.) and Shell, as well as the feedback and advice of principal scientists/engineers from each of these corporations and Combustion Engineering-ABB and Textron. We appreciate this level of collaboration, and expect that it will accelerate inevitable applications of our results in areas relevant to their technological objectives (see, also, Section 3.4, below).

3.3 Presentations and Research Training

Apart from the publications itemized in Section 5 and our verbal presentation (of progress) at the regular AFOSR Contractors Meetings , our results have also been presented at some 30 seminars/conferences--including annual or topical conferences of the following professional organizations:

Int. Fine Particle Res. Inst. (6/92, 6/93)
AIChE (11/91, 11/92, 11/93)
AAAR (10/93)
Electrochemical Soc. (CVD XI (5/91), XII; 5/20/93)
ASME-Engineering Foundation (3/91)
Materials Research Society
Combustion Inst.

In addition, during the period: 2/15/91-2/14/94, the PI presented seminars at the following Universities:

U Manchester 5/28/92	Leeds 5/29/92	Penn State (7/28/92)
Northwestern 4/22/93	CUNY 10/18/93	KTH-Stockholm
Brown (9/22/92)	Notre Dame (10/27/92)	U. Paris-Nord.
U. Wisconsin	U. Oslo	U. Limoges
Trondheim	U. Tolouse	Technion-Haifa
Waterloo		

This program involved completion of the PhD dissertation research of three Yale graduate students (J. Collins , A.G. Konstandopoulos and M. Tassopoulos; *cf.* Table 3.1-1) and will form the basis of the dissertation of P. Tandon (to be completed during '94-'95). Also, T. Kho has received her Master's Degree based on work supported in this program.

3.4 Some Known *Applications* of Yale-HTCRE Lab Research Results

It has been particularly gratifying to see direct applications of some of this generic AFOSR-supported particle and vapor mass transfer research in more applications-oriented

investigations reported in recent years. Indeed, *the writer would appreciate it if further examples known to the reader can be brought to his attention.*

Our AFOSR supported research on *soot deposition rates* from flowing laminar or turbulent combustion gases has been applied by Aerojet Corp. (D. Makel *et.al.*,1990) to develop a model for application to rocket chambers and nozzles (with NASA support). Extensions to jet engine nozzles are currently being made by M.T. Nys at Pratt and Whitney Engine Business in W. Palm Beach FL

In the area of multicomponent vapor deposition in combustion systems applications of our predictive methods (for "chemically frozen" (Rosner *et.al.*, 1979) and LTCE multicomponent laminar boundary layers) have been made by British Coal Corporation-Power Generation Branch (I. Fantom, contact) in connection with their topping cycles which run gas turbines on the products of fluidized bed coal combustors/gasifiers. Also, in combustion research many groups (*eg.*, Dobbins *et.al.* (Brown U.), Faeth *et.al.* (U. Mich.), Katz *et al.* (J. Hopkins U.)) are now utilizing "thermophoretic sampling" techniques to exploit the size- and morphology-insensitive capture efficiency characteristics that we have proven in our AFOSR research (Section 2.1).

Our AFOSR and NASA fundamental research on chemical element segregation in the CVD of refractory ceramics (*eg.*, SiC and metal borides) (see, *eg.*, Collins and Rosner, 1991, 1992) is evidently of use to AFML contractors synthesizing controlled stoichiometry fibers for light weight/high strength composites (Americom, Textron).

For calculating suspended particle concentrations along trajectories outside of aircraft (involved in atmospheric sampling), or inside of CVD reactors, A. S. Geller and D. J. Rader of Sandia-Albuquerque have adopted a method developed in our earlier AFOSR work (Fernandez de la Mora, 1981), and recently applied in our own studies of particle motion in laminar boundary layers with streamwise curvature (Konstandopoulos and Rosnert, 1994).

Ongoing work at MIT (Walsh *et.al.* 1992), PSI (J.J.Helble) and Sandia CRF (L.L. Baxter) has incorporated our rational correlation of *inertial particle impaction* (*e.g.* a cylinder in cross-flow) in terms of our *effective Stokes number* (Israel and Rosner, 1983, and Konstandopoulos *et. al.* 1993). Recent applications of our AFOSR and DOE-supported research (on the correlation of inertial impaction by cylinders in crossflow) have also been made by the National Engineering Laboratory (NEL) of Glasgow Scotland (Contact: Dr. A. Jenkins). NEL is apparently developing mass-transfer prediction methods applicable to waste-heat recovery systems in incinerators, as well as pulverized coal-fired boilers. These applications are somewhat similar to those reported by the Combustion R&D group at MIT and Penn State U, and are now being taken up by VTT-Energy/Aerosol Technology Group, in Finland.

Explicit use of our studies of self-regulated "capture" of incident impacting particles (Rosner and Nagaragan, 1987) is being made in current work on impact separators and ceramic heat exchangers for coal-fired turbine systems in high performance stationary power plants. Other potential applications arise in connection with "candle filters" used to remove fines (sorbent particles,...) upstream of the turbines. A useful summary of work in these interrelated areas (Solar Turbines, Textron Defense Systems, Hague International,...) was

presented at the Engineering Foundation Conference *Inorganic Transformations and Ash Deposition During Combustion.*, the proceedings of which appeared in 1992.

Clearly, fruitful *opportunities* for the application of our recent "non-Brownian" convective mass transfer research now exist in many of the programs currently supported by the US Air Force, as well as civilian sector R&D.

4. CONCLUSIONS

In the OSR-sponsored Yale HTCRE Lab research during the period: 2/15/91-2/14/94, briefly described above, we have shown that new methods for rapidly measuring particle-mass transfer rates, combined with our recent advances in mass transport theory, provide useful means to identify and incorporate important, but previously neglected, mass transport phenomena in many chemical propulsion engineering and materials engineering design/optimization calculations. One important class of examples involve our treatment of aggregated particle transport phenomena (Section 2.1)

Despite formidable complexities to be overcome in the design and operation of mobile and stationary power plants utilizing a broad spectrum of energetic fuels the abovementioned techniques and results (Section 2) are indicative of the potentially useful simplifications and generalizations emerging from our present fundamental AFOSR-funded research studies of combustion-generated particle transport mechanisms and interfacial reactions relevant to the synthesis of refractory materials. It is hoped that this Final Report and its supporting papers (Section 5) will facilitate the incorporation of many of the present ideas into design and test procedures of greater generality and reliability. This work has also helped identify new directions where it is anticipated that research results from this AFOSR program have a significant impact on future DOD and civilian sector engineering practice.

5. REFERENCES

5.1 CITED BACKGROUND PUBLICATIONS (Predecessor OSR, DOE-Grants)

Eisner, A.D. and Rosner, D.E., Experimental Studies of Soot Particle Thermophoresis in Non-Isothermal Combustion Gases Using Thermocouple Response Techniques", *Combustion and Flame* **61**, 153-166(1985); see, also: *J PhysicoChemical Hydrodynamics* (Pergamon) **7** , 91-100 (1986)

Fernandez de la Mora, J. and Rosner, D.E., "Inertial Deposition of Particles Revisited and Extended: Eulerian Approach to a Traditionally Lagrangian Problem", PCH *Physicochemical Hydrodynamics* (Pergamon) **2** (1), 1-21, (1981)

Geller, A.S., Rader, D.J. and Kempka, S.N., "Calculation of Particle Concentration Around Aircraft-Like Geometries", *J. Aerosol Sci.* **24** (6) 823-834 (1993)

Rosner, D.E. and Kim, S.S., "Optical Experiments on Thermophoretically Augmented Submicron Particle Deposition From 'Dusty' High Temperature Gas Flows", *The Chemical Engrg. J.*(Elsevier) **29**,[3], 147-157 (1984)

Rosner, D.E. and Nagarajan. R.,"Toward a Mechanistic Theory of Net Deposit Growth from Ash-Laden Flowing Combustion Gases: Self-Regulated Sticking of Impacting Particles and Deposit Erosion in the Presence of Vapor 'Glue'", *Proc. 24th National Heat Transfer Conf.*, AIChE Symposium Series, Vol. **83** [257], 289-296, (1987)

Rosner, D. E. , Chen, B.K., Fryburg, G.C. and Kohl, F.J., Chemically Frozen Multicomponent Boundary Layer Theory of Salt and/or Ash Deposition Rates from Combustion Gases", *Combustion Science and Technology* **20**, 87-106 (1979)

Rosner, D.E., **Transport Processes in Chemically Reacting Flow Systems**, Butterworth-Heinemann, Stoneham MA, 1986; 3d Printing 1990.

Rosner, D.E., Mackowski, D.W and Garcia-Ybarra, P., "Size and Structure-Insensitivity of the Thermophoretic Transport of Aggregated 'Soot' Particles in Gases", *Comb. Sci & Technology* **80** (1-3), 87-101 (1991).

Sung, C. J., Law, C. K., and Axelbaum, R. L., "Thermophoretic Effects on Seeding Particles in LDV Measurements of Flames", *Combustion Science and Technology* (submitted, 1993)

Walsh, P.M., Sarofim, A. F., and Beer, J.M., "Fouling of Convection Heat Exchangers by Lignitic Coal Ash", *Energy and Fuels* (ACS) **6** (6) 709-715 (1992)

5.2 PUBLICATIONS WHICH APPEARED* BASED IN PART ON GRANT AFOSR 91-0170

Castillo, J.L., Garcia-Ybarra, P., and Rosner, D.E.,"Morphological Instability of a Thermophoretically Growing Deposit", *J. Crystal Growth* **116**, 105-126, (1992)

Collins, J., Rosner , D. E. and Castillo, J.L., "Onset Conditions for Gas Phase Reaction and Nucleation in the CVD of Transition Metal Oxides", *Materials Research Soc. Symposium Proceedings* Vol. **250**, MRS (Pittsburgh PA) (1992), pp. 53-58

Collins, J., **Effects of Homogeneous Reaction on the Chemical Vapor Deposition of Titanium Dioxide**, PhD Dissertation, Yale University-Graduate School, Dept. Chemical Engineering, 1994

Rosner, D. E., Collins, J. and Castillo, J.L., "Onset Conditions for Gas Phase Reactions and Particle Nucleation/Growth in CVD Boundary Layers", in Proc. *Int. Conf. on CVD (XII)*, 1993, pp 41-47.

Gomez, A., and Rosner, D.E., "Thermophoretic Effects on Particles in Counterflow Laminar Diffusion Flames " *Combustion Science and Technology* **89**, 335-362 (1993)

Gomez, A., Rosner, D.E. and Zvuloni, R., "Recent Studies of the Kinetics of Solid Boron Gasification by $B_2O_3(g)$ and Their Chemical Propulsion Implications", *Proc. 2d Int. Sympos.*
on Special Topics in Chemical Propulsion: **Combustion of Boron-Based Solid Propellants and Solid Fuels**, (1992), pp 113-132.

---

*During this reporting period; Full papers for the 3d (final) year are reproduced in Section 6 (with Forms 298)

Rosner, D.E., Konstandopoulos, A.G., Tassopoulos, M., and Mackowski, D.W, "Deposition Dynamics of Combustion-Generated Particles: Summary of Recent Studies of Particle Transport Mechanisms, Capture Rates, and Resulting Deposit Microstructure/Properties", *Proc. Engineering Foundation Conference*: **Inorganic Transformations and Ash Deposition During Combustion**, Engrg. Foundation/ASME, NYC (1992); pp. 585-606

Konstandopoulos, A.G., Labowsky, M J., and Rosner, D.E., "Inertial Deposition of Particles From Potential Flows Past Cylinder Arrays", *J. Aerosol Sci* (Pergamon) **24** (4) 471-483 (1993)

Mackowski, D.W., Tassopoulos, M. and Rosner, D.E.,"Effect of Radiative Heat Transfer on the Coagulation Dynamics of Combustion-Generated Particles", *Aerosol Sci. Technol.(AAAR)* **20** (1) 83-99,(1993))

Rosner, D.E.and Tassopoulos, M.," Direct Solutions to the Canonical 'Inverse' Problem of Aerosol Sampling Theory: Coagulation and Size-dependent Wall Loss Corrections for Log-Normally Distributed Aerosols in Upstream Sampling Tubes", *J. Aerosol Sci.* **22** (7) 843-867 (1991).

Rosner, D.E., Mackowski, D.W,. Tassopoulos, M., Castillo, J.L., and Garcia-Ybarra, P., "Effects of Heat Transfer on the Dynamics and Transport of Small Particles in Gases", *I/EC -Research (ACS)* **31**,760-769 (1992)

5.3 PAPERS IN PREPARATION OR SUBMITTED FOR PUBLICATION

Albagli, D., Xing, Y. and Rosner, D.E., "Factors Governing the Accessible Surface Area of Combustion-Generated Ultrafine Particles" (in preparation, 1994)

Cohen, R. D., and Rosner, D. E. , "Kinetics of Restructuring of Large Multiparticle Aggregates"
(in preparation, 1994; Preliminary version presented at 10/93 AAAR Mtg.))

Castillo, J. L. and Rosner, D.E., Role of High Activation Energy Homogeneous Chemical Reactions in Affecting CVD-Rates and Deposit Quality for Heated Surfaces", in preparation
for *Chem Eng. Sci.*, 1994)

Konstandopoulos, A.G. and Rosner, D.E.,"Inertial Effects on Thermophoretic Transport of Small Particles to Walls With Streamwise Curvature---I. Experiment, II. Theory", Accepted 1993 and in press, *Int. J. Heat Mass Transfer* (Pergamon)

Kho, T. , Collins, J. and Rosner, D. E., "Development, Preliminary Testing, and Future Applications of a Rational Correlation for the Grain Densities of Vapor-Deposited Materials"
(in preparation for submission to *J. Materials Sci.*, 1994)

Kho, T., Rosner, D.E., and Tandon, P., "Simplified Erosion Rate Prediction Technique for Cylindrical Targets in the High Speed Crossflow of Abrasive Suspensions", (in preparation, for submission to *ASME Trans-J. Engrg. Gas Turbines and Power*, 1994)

Park, H.M., and Rosner, D.E., "Thermophoretically Induced Phase Separation in Highly-Loaded 'Dusty' Gas Mixtures" (Revised version of HTCRE #162, revision in preparation 1994)

Rosner, D.E. and Tandon, P., "Diffusion and Heterogeneous Reaction in Large Multi-particle Aggregates; Calculation and Correlation of 'Accessible' Surface Area", (accepted; to appear *AIChE J.* summer '94)

Rosner, D.E., Tandon, P. and Konstandopoulos, A.G., "Rational Prediction of Inertially Induced Particle Deposition Rates for a Cylindrical Target in Dust-Laden Streams", (in preparation, to be submitted to *Chem. Eng. Sci.*, summer 1994); see, also: Proc. 1st Int. Particle Technology Forum, AIChE (in press, 1994).

Rosner, D. E., Tandon, A.G., and Konstandopoulos, A.G., "Local Size Distributions of Particles Deposited by Inertial Impaction on a Cylindrical Target in Dust-Laden Streams", (in preparation, to be submitted to *J. Aerosol Sci.*, 1994)

Rosner, D.E., Tassopoulos M., and Tandon, P. , "Sensitivity of Total Mass Deposition Rate and Resulting Deposit Microstructure to Morphology of Coagulation-Aged Aerosol Populations of Aggregated Primary Particles", in preparation, 1994)

Zvuloni, R., Rosner, D.E., and Gomez, A., "High Temperature Kinetics of Solid Boron Gasification By its Higher Oxide $B_2O_3(g)$: Flow Reactor Techniques, Rate Measurements and Their Chemical Implications", *J. Phys. Chem.* (to be submitted, 1994)

LIST OF ABBREVIATIONS

BL	Boundary layer	CDF	Counterflow diffusion flame
CVD	Chemical vapor deposition	CRF	Combustion Research Facility
Dam	Damköhler number	CSL	Chemical sublayer
G/S	Gas/solid interface	GRA	Graduate research Asst.
IJHMT	Int. J. Heat/Mass Xfer	PSD	Particle size distribution
LDV	Laser Doppler Velocimetry	LTCE	local thermochemical equilibrium
MRS	Materials Research Society	TTIP	Titanium tetra-isopropoxide
TEM	Transm. Electron μ-scope	*pdf*	Probability density function

6. APPENDICES (Complete Papers Published During 2/15/93-2/14/94 Period; including Form 298 for each)

REPORT DOCUMENTATION PAGE

Form Approved
OMB No. 0704-0188

1. AGENCY USE ONLY (Leave blank)	2. REPORT DATE	3. REPORT TYPE AND DATES COVERED
	1994	Reprint: Aerosol Sci. Tech. 20, 83-99

4. TITLE Effect of Radiative Heat Transfer on the Coagulation Dynamics of Combustion-Generated Particles

5. FUNDING NUMBERS

PE - 61102F
PR - 2308
SA - BS
G - 91-0170 (AFOSR)

6. AUTHOR(S)

Daniel W. Mackowski, Menelaos Tassopoulos and Daniel E. Rosner

7. PERFORMING ORGANIZATION NAME(S) AND ADDRESS(ES)

HIGH TEMPERATURE CHEMICAL REACTION ENGINEERING LABORATORY
YALE UNIVERSITY
BOX 208286 YALE STATION
NEW HAVEN, CONNECTICUT 06520 U.S.A.

8. PERFORMING ORGANIZATION REPORT NUMBER

9. SPONSORING/MONITORING AGENCY NAME(S) AND ADDRESS(ES)

AFOSR/NA
Building 410
Bolling AFB DC 20332-6448

10. SPONSORING/MONITORING AGENCY REPORT NUMBER

11. SUPPLEMENTARY NOTES

12a. DISTRIBUTION/AVAILABILITY STATEMENT

Approved for public release; distribution is unlimited

12b. DISTRIBUTION CODE

13. ABSTRACT (Maximum 200 words)

We examine the influences of radiation heat transfer on the size and number density evolution of small coagulating particles. On a microscopic level, radiative emission and/or absorption by the particle will perturb the gas temperature field adjacent to each particle. As a result of thermophoretic particle transport, the nonequilibrium condition can alter the collision rates with neighboring particles. A simplified analysis of the thermophoretic coagulation mechanism suggests that net radiative cooling of the particles can lead to an accelerated growth of μm-sized particles, whereas net radiative heating can act to essentially freeze coagulation rates. On the macroscopic level, the addition or removal of heat in the gas through radiative absorption/emission by the particle cloud can also significantly alter, through thermophoretic transport, the local particle number density. Under certain cases these effects can augment the accelerated coagulation rates that occur under radiative cooling conditions. We also examine the particular situation of equilibrium between particle cloud radiative absorption and emission—which results in no net macroscopic effect on the gas. Under conditions where the spectral distribution of the incident radiation differs from that of the emitted radiation, radiative equilibrium can lead to accelerated growth of certain particle sizes and retarded growth of others. Using numerical solutions to the general dynamic equation for particle growth, we demonstrate the possibility of using incident radiation of controlled intensity and spectral distribution to narrow the particle size distribution function of coagulating aerosols.

14. SUBJECT TERMS

Key words. Soot, aggregated particles, mass transport, thermophoresis, agglomerates; Brownian diffusion.

15. NUMBER OF PAGES
9

16. PRICE CODE

17. SECURITY CLASSIFICATION OF REPORT	18. SECURITY CLASSIFICATION OF THIS PAGE	19. SECURITY CLASSIFICATION OF ABSTRACT	20. LIMITATION OF ABSTRACT
Unclassified	Unclassified	Unclassified	UL

AEROSOL SCIENCE AND TECHNOLOGY
THE JOURNAL OF THE AMERICAN ASSOCIATION FOR AEROSOL RESEARCH
AAAR Office, 6500 Glenway Avenue, Building D-7, Cincinnati, OH 45211-4438 Phone (513) 661-3385

VOLUME 20, NUMBER 1, 1994

CONTENTS

#183

Effect of Radiative Heat Transfer on the Coagulation Dynamics of Combustion-Generated Particles

Daniel W. Mackowski*
Mechanical Engineering Department, Auburn University, AL 36849

Menelaos Tassopoulos and Daniel E. Rosner
High Temperature Chemical Reaction Engineering Laboratory, Chemical Engineering Department, Yale University, New Haven, CT 06520-8286

We examine the influences of radiation heat transfer on the size and number density evolution of small coagulating particles. On a microscopic level, radiative emission and/or absorption by the particle will perturb the gas temperature field adjacent to each particle. As a result of thermophoretic particle transport, the nonequilibrium condition can alter the collision rates with neighboring particles. A simplified analysis of the thermophoretic coagulation mechanism suggests that net radiative cooling of the particles can lead to an accelerated growth of μm-sized particles, whereas net radiative heating can act to essentially freeze coagulation rates. On the macroscopic level, the addition or removal of heat in the gas through radiative absorption/emission by the particle cloud can also significantly alter, through thermophoretic transport, the local particle number density. Under certain cases these effects can augment the accelerated coagulation rates that occur under radiative cooling conditions. We also examine the particular situation of equilibrium between particle cloud radiative absorption and emission—which results in no net macroscopic effect on the gas. Under conditions where the spectral distribution of the incident radiation differs from that of the emitted radiation, radiative equilibrium can lead to accelerated growth of certain particle sizes and retarded growth of others. Using numerical solutions to the general dynamic equation for particle growth, we demonstrate the possibility of using incident radiation of controlled intensity and spectral distribution to narrow the particle size distribution function of coagulating aerosols.

I. INTRODUCTION

It is well known that small aerosol particles can profoundly affect radiative energy transfer in high temperature environments. Indeed, in combustion situations the contribution of particle radiative emission to the net heat transfer is often significant—if not dominant—and a vast amount of theoretical and experimental research has been devoted to examining the influence of particles on radiation (see, e.g., Viskanta and Menguç, 1987).

On the other hand, relatively few investigations of the influence of radiation heat transfer on particle dynamics have been performed. In previous work, we addressed the effects of both radiative and conductive heat transfer on the transport of small particles suspended in gases (Mackowski, 1990; Rosner et al., 1992). In this article we focus on the relationship

*To whom correspondence should be addressed.

Aerosol Science and Technology 20:83–99 (1994)
© 1994 Elsevier Science Inc.

83-99

0278-6826/94/$7.00

between radiation and the coagulation dynamics of sub to near-μm particles. For particles of this size Brownian motion has been commonly identified as the dominant mechanism for bringing together initially separated particles. Since the pioneering work of Smoluchowski (1917), there have been many theoretical studies of the evolution of particle size due to Brownian coagulation, either acting alone (Friedlander and Wang, 1966; Lee, 1983) or in concert with other processes (Megaridis and Dobbins, 1989; Tsang and Rao, 1988; Rosner and Tassopoulos, 1991).

Radiation will affect particle coagulation dynamics by altering the temperature field in the gas on both microscopic (i.e., particle–particle) and macroscopic (particle cloud) levels. On the microscopic level the emission or absorption of radiation by the particle will be balanced by conduction heat transfer between the particle and the local gas. The particle and gas will thus be in a state of thermal nonequilibrium, and a gas temperature gradient will extend outward from the particle. The gradient, through the transport mechanism of thermophoresis, will alter the collision rates with neighboring particles. This phenomenon is familiar to anyone who has immersed a thermocouple bead (or any small object) into a sooting flame (Eisner and Rosner, 1985). Because of radiative emission, the bead will be cooler than the gas, and thermophoresis will quickly result in the fouling of the bead by soot particles. Radiation-induced thermophoretic coagulation among particles is essentially the same—except that the particles deposit on each other instead of a thermocouple bead.

Researchers in the field of atmospheric aerosols have recognized for some time that thermophoretic coagulation can play a significant role in the scavenging of small particles by water droplets—in which the droplet heat "sink" occurs not from radiative transfer but from the latent heat of vaporization (Hampl et al., 1971; Slinn and Hales, 1971; Wang et al., 1983). In section 3, we perform an analysis of radiation-modified particle coagulation, and demonstrate its potential significance in affecting the growth of μm-sized particles in high-temperature environments.

Radiation-induced thermophoresis can also have an effect on the macroscopic, or bulk properties of the particle cloud. The mechanisms on this scale are connected to the response of the bulk gas to the energy transfer from particle emission or absorption. For example, under overall steady-state conditions the net transfer of energy from the gas via particle emission will be balanced by conduction of heat into the gas from its boundaries. The gas temperature gradients arising from the conduction heat transfer will lead to a thermophoretic transport of particles into the interior regions of the gas. In section 4 we present a simplified analysis of the macroscopic effects of radiation on particle concentration, and contrast the effects with those arising on the microscopic level.

Generally, it is not possible to predict the effects of microscopic-level thermophoretic coagulation on the particle size evolution without also considering the macroscopic effects of radiation on the bulk gas. We examine in section 5 a particular situation in which this is not the case—namely, radiative equilibrium. In this case, the net transfer of heat to or from the gas by the particles will be zero. However, we demonstrate that if the absorbed radiative energy spectrum differs from the emitted spectrum, most of the individual particles can still be in some degree of thermal nonequilibrium with the gas. As a result, certain particle sizes can experience accelerated growth, and other sizes will have retarded growth. With an eye toward manipulating the particle size distribution (PSD) spectrum, we perform numerical solutions of the general dynamic equation for particle coagulation in section 6, and show that, for a suitable choice of incident radiation, coagulation can act in radiative equilibrium conditions to actually narrow the particle size distribution.

2. RADIATIVE MODEL

We begin our analysis by formulating the radiative energy transfer through absorption and emission by an individual particle. Let $\dot{Q}$ denote the net energy transfer rate to the particle. Assuming that the particle is at a uniform temperature T, $\dot{Q}$ can be written simply as the difference between the absorption and emission rates of the particle, that is,

$$\dot{Q} = \dot{Q}_{\text{abs}} - \dot{Q}_{\text{emis}} = \bar{C}_a G - 4\pi \bar{C}_e \sigma T^4 \tag{1}$$

in which G denotes the total incident radiation per unit area within the medium, σ is the Stefan-Boltzmann constant, and $\bar{C}_a$ and $\bar{C}_e$ are the total absorption and emission cross sections of the particle, defined by

$$\bar{C}_a = \frac{1}{G}\int_0^\infty G_\lambda C_a \, d\lambda \tag{2}$$

$$\bar{C}_e = \frac{1}{\sigma T^4}\int_0^\infty e_{b\lambda}(T) C_a \, d\lambda \tag{3}$$

where λ denotes wavelength, G_λ and $e_{b\lambda}(T)$ are the spectral incident radiation and blackbody emissive power, respectively, and C_a is the spectral absorption cross section of the particle. For spherical, homogeneous particles of radius a, C_a is predicted from Lorenz/Mie theory as a function of the size parameter $x = 2\pi a/\lambda$ and the (wavelength-dependent) complex refractive index $m = n + ik$ (Bohren and Huffman, 1983). Of course, "real" aerosol particles are seldom spherical in shape. Carbonaceous soot, for example, forms as aggregates of small (≈ 0.02 μm) spheres (Megaridis and Dobbins, 1989). For such particles it has been suggested (Drolen and Tien, 1986) that the absorption cross section can be well approximated by that of an "equivalent" Lorenz/Mie sphere having the same volume as the aggregate. In our calculations we will thus take the particle radius a to correspond to the volume-mean radius of the particle, and use Lorenz/Mie theory to estimate the absorption cross section.

In general, prediction of the incident radiation G_λ is accomplished through solution of the radiative transfer equation—which takes into account the emission and scattering of radiation from all the other particles in the system, as well as radiation incident at the system boundaries (Sparrow and Cess, 1978). Such an analysis is not the intention of the work presented here. Instead, we assume that the particle cloud can be radiatively characterized as optically thin—which implies that the contribution to G_λ of emitted and scattered radiation from other particles is negligible—and take G_λ to be entirely due to radiation of a known spectral distribution originating external to the particle cloud system.

For the examples given in subsequent sections, we will assume that G_λ is characterized either as a greybody radiating at an environment temperature T_{env} with an emittance ϵ_{env}, or as a monochromatic source at wavelength λ_i. A further approximation to the expression for $\dot{Q}$ makes use of the fact that, for μm-sized particles at combustion temperatures, the difference between the particle temperature and the neighboring bulk gas temperature will be on the order of only a few K. Because it will be the magnitude of $\dot{Q}$, rather than the actual particle-gas temperature difference, that will be the determining factor in the thermophoretically induced coagulation effects, it is appropriate to assume that the particles radiate at the local gas temperature T_g.

Also, in keeping with the combustion-particle focus of this work, we will take the optical properties of the particles to be characteristic of carbonaceous soot. Rather than employing a wavelength-dependent refractive index m in our numerical computations of Eq. (3), we use a constant value corresponding to that predicted, from dispersion relations (Lee and Tien, 1981), at the wavelength of peak emission at the corresponding temperature, that is, $\lambda = 2898\ \mu\text{m K}/T_g$.

3. THERMOPHORETIC COAGULATION

We now examine the effect of the radiative transfer rates $\dot{Q}$ on a pair of neighboring particles. The particles, denoted 1 and 2, are initially separated by a distance R that is taken to be significantly greater than the mean-free-path of the gas molecules. We neglect higher-order thermal and hydrodynamic interactions between the particles, and take the gas to be in a locally quiescent, quasi-steady state. We also assume that "bulk" transport mechanisms of the particles, such as thermophoresis from a temperature gradient in the bulk gas, photophoresis and gas convection, do not result in a significant relative velocity between the particles. From energy conservation, particle 2 will experience a continuum gas temperature gradient resulting from energy transfer from particle 1 equal to,

$$\left.\frac{dT_g}{dr}\right|_2 = -\frac{\dot{Q}_1}{4\pi R^2 k_g} \tag{4}$$

where the coordinate r is taken from particle 1 to 2. The gas temperature gradient will result in a thermophoretic motion of particle 2. Phenomenologically, the thermophoretic velocity V_T can be related to the gradient by the equation (Talbot et al., 1980; Rosner, 1986)

$$V_T = -\frac{C_T \nu}{T_g}\frac{dT_g}{dr}. \tag{5}$$

In the above, ν is the gas kinematic viscosity and C_T is a dimensionless parameter. Estimation of C_T must take into account, among other things, the Knudsen number $Kn = l/a$ of the particle, where l is the mean-free-path of the gas molecules and a is the characteristic particle size. Closed-form expressions for C_T can be obtained in the free molecule ($Kn \to \infty$) and slip-flow ($Kn \ll 1$) regimes. Although an exact solution or C_T in the $Kn \approx 1$ regime is generally not tractable, Talbot et al. (1980) found that the fitting formula,

$$C_T = \frac{2c_s(\kappa + c_t Kn) f_C}{(1 + 3c_m Kn)(1 + 2\kappa + 2c_t Kn)} \tag{6}$$

yields values that are in reasonable agreement with available experimental results for the entire range of Kn. In the above, $\kappa \equiv k_g/k_p$ is the ratio of gas and particle thermal conductivities, c_s, c_t, and c_m are coefficients of thermal slip, temperature jump, and velocity jump, with values (for complete thermal and momentum accommodation) of 1.17, 2.18, and 1.14, respectively, and f_C is the Cunningham slip correction factor given by

$$f_C = 1 + Kn(A + Be^{-C/Kn}) \tag{7}$$

in which the values of the constants A, B, and C may be taken to be 1.20, 0.41, and 0.88, respectively (Loyolka and Cipolla, 1971; Talbot et al., 1980).

Using Eqs. (4) and (5), and analogous relations for particle 1, the net rate at which the particles move toward (or away from) each other will be

$$V_{T,1} + V_{T,2} = \left[(C_T)_1 \dot{Q}_2 + (C_T)_2 \dot{Q}_1\right] \times \frac{\nu}{4\pi R^2 k_g T_g}. \tag{8}$$

The motion is *as if* an attractive (or repulsive) force acted between the two particles, of magnitude

$$F_T(R) = \frac{V_{T,1} + V_{T,2}}{B_1 + B_2} \tag{9}$$

where B_1 and B_2 are the particle mobilities (reciprocal of drag force per unit velocity) in the surrounding gas. For spherical particles, B is given by

$$B = \frac{1 + Kn(A + Be^{-C/Kn})}{6\pi\mu a} \tag{10}$$

where μ is the dynamic viscosity of the gas.

Inspection of Eqs. (8) and (9) reveal that the "effective" thermophoretic force F_T is proportional to R^{-2}. Because of the inverse-square dependence, the analysis at this point can borrow from the thoroughly investigated phenomenon of coagulation between *electrically charged* particles (Zebel, 1966; Friedlander, 1977). It is important to emphasize, however, that the effective thermophoretic force is not precisely equivalent to the instantaneous force acting over a distance in electrostatics. In thermophoresis, the "action" between the particles must be propagated (as heat transfer) through the carrier gas. A true inverse-square relationship would be expected only if the characteristic time of gas heat transfer propagation was considerably smaller than the characteristic time of particle motion. From a simple dimensional analysis, the ratio of gas and particle characteristic times will be on the order of $C_T Pr$, where $Pr = \rho c_p \nu/k_g$ is the Prandtl number of the gas and ρ and c_p are the gas density and constant-pressure specific heat, respectively. For μm-sized particles in air, $C_T Pr$ will be on the order of 0.1, which is not, strictly speaking, infinitesimal, but small enough to justify an inverse-square approximation as a first estimate of thermophoretic coagulation effects.

Therefore, from the electrical analogy, the ratio of coagulation rate constants between particles 1 and 2 including thermophoresis to that due to Brownian motion alone, denoted Z, can be expressed as (Zebel, 1966; Friedlander, 1977)

$$Z(a_1, a_2) = \frac{y}{e^y - 1}. \tag{11}$$

In the above,

$$y = \frac{F_T(a_{12})a_{12}}{k_B T_g} \tag{12}$$

where $a_{12} = a_1 + a_2$ is the separation distance at contact, and k_B is Boltzmann's constant. When the energy transfer rates $\dot{Q}$ are negative (such as in radiative cooling), the thermophoretic force F_T is negative and the correction factor Z exceeds unity, as expected. Particles hotter than the gas have a Z-factor less than unity.

For purposes of illustration, we present in Figure 1 a plot of Z versus particle radius a_1 with a_2 as a parameter, and calculated for conditions of net radiative heating and net radiative cooling. The incident radiation G is taken to correspond to a blackbody at $T_{env} = 1050$ and 950 K, and the gas temperature T_g is 1000 K. The gas is taken to be air at 1 atm pressure. The onset of the thermophoretic effects are seen to occur, for these particular radiative conditions, for radii in the range of 0.1–1 μm. Under conditions of

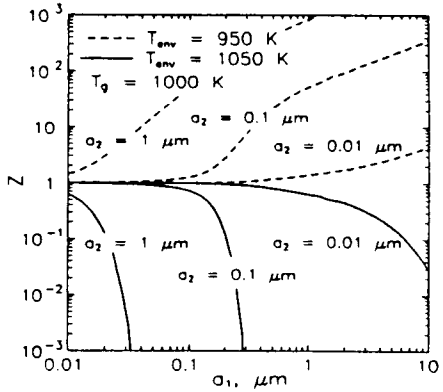

FIGURE 1. Thermophoretic coagulation factor.

radiative cooling (T_{env} = 950 K), the growth of relative large (≈ 1 μm) particles will be tremendously accelerated in comparison to pure Brownian coagulation. Radiative heating (T_{env} = 1050 K), on the other hand, will act to retard or arrest the growth of the larger particles.

4. MACROSCOPIC ANALYSIS OF RADIATION / PARTICLE INTERACTIONS

The results of the previous section suggest that radiative absorption or emission by the particles could have a considerable effect on particle coagulation. However, the transfer of radiation to or from the particle cloud will lead to a bulk heating or cooling of the gas, which in turn will have direct bearing on the particle dynamics. In this section we examine the effects of the macroscopic-level energy transfer on particle concentration. We begin by formulating a simplified energy equation for the gas. Assuming the particles have negligible influence on the thermophysical properties of the gas and that the gas itself does not absorb or emit radiation, gas phase energy conservation is expressed

$$\rho c_p \left[\frac{\partial T_g}{\partial t} + \mathbf{v} \cdot \nabla T_g \right] = k_g \nabla^2 T_g + q''' \qquad (13)$$

where $\mathbf{v}$ denotes the convective velocity of the gas, and q''' is the volumetric heat source resulting from particle radiative transfer. Considering the general case of a polydispersion of particles represented by a normalized PSD function $f(a)$, the heat source is given by

$$q''' = N_p \int_0^\infty \dot{Q} f(a)\, da. \qquad (14)$$

The coupling of the particle concentration to the gas energy equation is clear—in that q''' is proportional to particle number density N_p. Prediction of N_p requires one to consider not only particle coagulation, but also convective, diffusive, and thermophoretic transport of the particles through the gas. The transport effects can be analyzed separately of the coagulation effects by examining the particle volume fraction ϕ, which will be unaffected by coagulation. Assuming that particle "sources" or sinks (nucleation, surface growth and oxidation) are absent, particle transport via inertial and gravitational forces is negligible, and gas density is constant, the conservation equation for particle volume fraction can be written

$$\left[\frac{\partial \phi}{\partial t} + \mathbf{v} \cdot \nabla \phi \right] = \nabla \cdot \left(D \nabla \phi + \frac{C_T \nu \phi}{T_g} \nabla T_g \right) \qquad (15)$$

in which D is the Brownian diffusion coefficient.

As was the case for the microscopic-level effects, thermophoresis on the macroscopic scale provides the mechanism through which particle radiative transfer can influence particle concentration. The ultimate contribution of radiation to the fate of the particles will obviously depend a great deal on factors such as the flow field, radiative environment, boundary and initial conditions of the system, etc. For practically all conceivable situations, solution of the temperature and particle mass fraction fields will require numerical methods—and such an analysis is beyond the scope of the present work. However, a limiting situation that provides insight to the macroscopic radiation-particle concentration linkage can be addressed directly.

Consider a volume of quiescent, particle-laden gas in which the bulk gas temperature at each point in the volume is steady. To maintain this condition, heat conduction into or from the gas at the boundaries of the volume must balance the net radiation transfer by the particles. Initially, the particles are assumed to be uniformly distributed throughout the volume. Taking the particles to be monodisperse, the energy equation reduces to

$$k_g \nabla^2 T_g = -N_p \dot{Q}. \qquad (16)$$

To simplify Eq. (15), we first neglect Brownian diffusion and approximate the quantity $C_T \nu / T_g$ as a constant. We then focus our attention in the interior regions of the volume, in which ϕ can be taken to be locally uniform. The preceeding assumptions lead to

$$\frac{d\phi}{dt} = \frac{C_T \nu \phi}{T_g} \nabla^2 T_g. \qquad (17)$$

Combining the above with the simplified energy equation, and using the relation $\phi = N_p \bar{v}$, where $\bar{v}$ is the mean particle volume, yields

$$\frac{d\phi}{dt} = -\frac{C_T \nu \dot{Q}}{\bar{v} k_g T_g} \phi^2 \qquad (18)$$

The case of net radiative absorption ($\dot{Q} > 0$) leads to a dispersal of the particles which is analogous to the phenomena of electrostatic dispersion experienced by like-charged particles (Zebel, 1966). Radiative cooling, on the other hand, results in a "compression" of the particles, in that the gradients tend to draw the particles together and thereby increase ϕ. The macroscopic-level effects, in this situation, would thus act to further enhance the microscopic-level coagulation effects. Because of particle coagulation, $\bar{v}$ and $\dot{Q}$ would not be constant. However, if the sizes of the particles are small with respect to the radiation wavelengths (i.e., the Rayleigh regime), the quantity $\dot{Q}/\bar{v}$ can be taken to be constant. Formally integrating Eq. (18) results in

$$\frac{\phi}{\phi_0} = \left[1 - \frac{t}{t_d} \right]^{-1} \qquad (19)$$

in which subscript 0 denotes the initial state, and the characteristic dispersion time t_d is

$$t_d = -\frac{\bar{v}_0 k_g T_g}{C_T \nu \dot{Q} \phi_0}. \qquad (20)$$

To give an idea of a typical value of t_d, assume a population of 0.1 μm particles with a volume fraction ϕ of 10^{-6}—corresponding to typical values of carbonaceous soot in flames (Viskanta and Menguç, 1987; Santoro et al., 1983). At a gas temperature of 1500 K and a blackbody environment at 1000 K, t_c will be on the order of 1 sec. This suggests that the bulk radiative cooling of a particle-laden gas could lead to an "explosive" increase in particle volume fraction.

In "real" combustion-environment systems, radiative heat transfer from the gas will also act to decrease the gas temperature, and thereby reduce the "driving force" behind the radiative-induced coagulation and dispersion mechanisms. For example, if the boundaries of the volume containing the particles and gas were adiabatic (as opposed to isothermal in the case above), and the particle concentration and temperature of the volume were initially uniform, radiative heat transfer from the gas would lead simply to a uniform cooling of the gas. No gradients would be induced in the gas, and consequently no particle dispersion would occur. It thus appears clear that the net effect of radiation heat transfer on the particle cloud properties will depend a great deal on the thermal boundary conditions of the gas-particle system.

In addition, the initial conditions of the system will also play an important role. In real situations, the initial particle concentration would not be uniform. Rather, the particles would be unevenly distributed in space. Regions containing a larger concentration of particles would experience a greater heat loss rate through radiation. This, in turn, would set up temperature gradients in the gas which would act to drive additional particles into the high-

concentration regions—that is, particle compression—and thereby accelerate the coagulation. In this sense, the radiation cooling/particle dynamics problem resembles a stability problem—in that particle concentration nonuniformities would tend to become amplified. A preliminary analysis of this phenomenon has recently been performed by Vedha-Nayagam and Mackowski (1992).

5. COAGULATION UNDER RADIATIVE EQUILIBRIUM

We examine now an interesting particular case of the energy balance expressed in Eq. (13). The particles are now taken to be in a net emission/absorption equilibrium condition, that is,

$$q''' = 0. \tag{21}$$

In addition, the gas temperature is assumed to be steady and uniform within the system. Under the optically thin conditions, the equilibrium condition requires that the total external radiation absorbed by the particles equals the total emitted radiation. As before, it is reasonable to approximate the particle emission temperature as the local bulk gas temperature. The radiative equilibrium condition is then expressed by the balance,

$$\int_0^\infty \left[G\bar{C}_a(a) - 4\pi\sigma T_g^4 \bar{C}_e(a, T_g)\right] \times f(a)\, da = 0. \tag{22}$$

For a given PSD function $f(a)$ and spectral characteristics of the incident radiation G_λ and particle optical properties m_λ, the above integral equation will provide a relation between the total incident radiation G and the gas temperature T_g. Note that, in general, the solution will not be equivalent simply to $G\bar{C}_a = 4\pi\sigma T_g^4 \bar{C}_e$, unless the incident radiation corresponds to a blackbody at temperature T_{env}, for which T_g will equal T_{env}, or the PSD function is represented by a delta function (i.e., the particles are monodisperse). The implication of this is that the individual particles can be in some degree of thermal nonequilibrium with the gas—some absorbing more radiation than emitting, some emitting more than absorbing—yet the particle cloud as a whole exchanges zero *net* energy to the gas. Under this condition thermophoretic coagulation mechanisms could affect the PSD evolution of the particle cloud, yet the bulk gas temperature could remain in a steady state condition.

Actually, if the total incident radiation G is fixed, then the gas temperature will change as the PSD function changes to maintain the balance expressed in Eq. (22). However, the temperature response time can be expected to be significantly smaller than the characteristic coagulation time, and the gas temperature could thus be taken to be quasi-steady.

The consequences on the PSD evolution of the radiation equilibrium condition appear to be especially intriguing. If, by a suitable choice of the incident radiation intensity and spectral distribution, the larger particles experienced a net radiative absorption, which would be balanced by the smaller ones having net radiative emission, then the coagulation rates of the larger and smaller particles would be retarded and accelerated, respectively. The PSD function of the coagulating particles would then narrow with time. If this condition was maintained, then the ultimate PSD function satisfying Eq. (22) (as mentioned above) would be a monodispersion. On the other hand, if the smaller particles were heated, yet the larger ones cooled, then the PSD function would broaden with time.

To give an illustration of the dependence of the individual particle heat source function on the characteristics of the PSD function and incident radiation, we first assume that the PSD can be represented by a log-normal form (Friedlander, 1977), that is,

$$f(a) = \frac{3}{\sqrt{2\pi}\, a \ln \sigma_g} \times \exp\left[-\frac{9}{2}\left(\frac{\ln(a/a_g)}{\ln \sigma_g}\right)^2\right]. \tag{23}$$

To contrast effects due to the spectral distribution of incident radiation, G is taken to be monochromatic at wavelengths of either 10.2 or 0.5145 μm—corresponding to CO_2 and Ar-ion laser sources, respectively. The gas temperature and σ_g are fixed at 600 K and 2.2, and, for a given a_g, the value of G satisfying radiative equilibrium is calculated through quadrature of Eqs. (3) and (22). For the 10.2 μm case, G varied from around 15 to 20 W/cm^2 for a_g ranging from 0.05 to 2 μm. At 0.5145 μm, G varied from 0.7 to 13 W/cm^2 for the same range of a_g. The results of the calculation are presented in Figures 2 and 3, in which the dimensionless particle heat source function, defined by,

$$f_Q(a) = \dot{Q}(a) f(a) \times \left\{\int_0^\infty \dot{Q}_{emis}(a') f(a')\, da'\right\}^{-1} \tag{24}$$

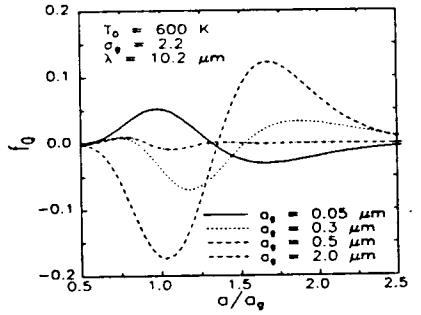

FIGURE 2. Dimensionless particle heat source function, 10.2 μm radiation.

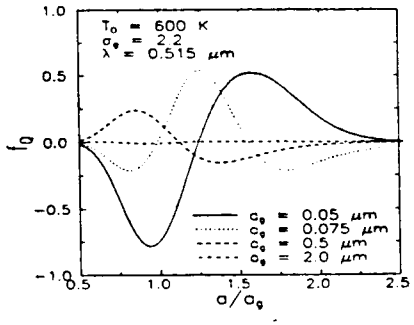

FIGURE 3. Dimensionless particle heat source function, 0.5145 μm radiation.

is plotted versus a/a_g with the geometric mean radius a_g as a parameter. As its definition indicates, f_Q gives the distribution of radiative heating/cooling rates among the particles, weighted by the particle size distribution function.

Several interesting features can be observed in the plots. For the 10.2 μm results, the f_Q values at $a_g = 0.05$ μm are negative for the larger particles and positive for the smaller. As discussed above, thermophoretic coagulation would act to accelerate the large particle growth relative to the small particle growth in this situation, with the net result of a broadening of the PSD. At $a_g = 0.3$ μm, one sees that the f_Q distribution has become bimodal, with both the largest and the smallest particles heated, and the intermediate ones cooled. As a_g increases to 0.5 μm, the distribution shifts to the opposite extreme—in that the large particles become heated. The PSD evolution under thermophoretic coagulation would now tend toward a narrower spectrum—because the growth of the largest particles will be arrested. Increasing a_g further to 2.0 μm results in a return of the bimodal f_Q distribution, although the magnitude of the particle heating or cooling (and hence the coagu-

lation "driving force") has been considerably reduced.

The trends for the 0.5145 μm results are qualitatively opposite to those for the longer wavelength. At $a_g = 0.05$ μm, the largest particles in the distribution are heated and the smallest particles are cooled. Coagulation among the larger particles would thus be inhibited. However, increasing the mean particle size slightly results in a bimodal distribution of f_Q. Large particle growth would now be accelerated. As a_g increases further, the larger particles remain cooled. It would thus appear that, for the short wavelength, thermophoretic coagulation would act to continuously broaden the PSD and increase the mean particle size.

To obtain a more quantitative analysis of the effect of radiative equilibrium on PSD evolution, numerical solutions of the general dynamic equation (GDE) for particle growth were undertaken. Under conditions where coagulation is the only growth mechanism (i.e., no surface growth or nucleation), and with particle volume rather than radius as the internal coordinate, the GDE can be written for a continuous PSD function as (Zebel, 1966; Friedlander, 1977)

$$\frac{\partial n(v)}{\partial t} = \frac{1}{2}\int_0^v \beta(u, v-u)n(v-u)n(u)\,du - n(v)\int_0^\infty \beta(u,v)n(u)\,du \quad (25)$$

where v and u represent particle volume and $n(v) = N_p f(v)$ is the particle number density distribution function. The first term in the above equation represents the creation of particles of volume v due to the coagulation between pairs of particles having volumes that sum to v. The second term represents the loss of particles of volume v due to coagulation between particles of volume v and all other particles.

In the following calculations of PSD evolution under radiative equilibrium, we will retain the spherical particle approximation in calculating the coagulation rate constants β. Again, "real" aerosol particles are seldom spherical in shape, especially those formed in combustion processes (e.g., soot aggregates). Although, as mentioned in section 2, the radiative absorption cross section of a nonspherical particle can be approximated by that of a spherical particle having the same volume, one would generally not expect the same equivalence with respect to the coagulation rate constants β. Considering, however, that our calculations are intended to provide a preliminary estimation of the effect of radiative equilibrium on PSD evolution, it is appropriate to begin with a broadly simplified representation of the rate constants.

The particle sizes of interest in this investigation will generally fall into the near-continuum Knudsen regime. Therefore, the harmonic average approximation for the coagulation kernel β is adopted (Sitarski and Seinfeld, 1977; Sceats, 1986), that is,

$$\beta = Z \cdot \frac{\beta_{FM}\beta_C}{\beta_{FM} + \beta_C} \quad (26)$$

in which β_{FM} and β_C denote the Brownian coagulation rates for spherical particles in the free-molecular and continuum regimes, and are given by,

$$\beta_{Fm} = \left(\frac{3}{4\pi}\right)^{1/6}\left(\frac{6k_BT}{\rho_p}\right)^{1/2} \times \left(\frac{1}{u} + \frac{1}{v}\right)^{1/2}(u^{1/3} + v^{1/3})^2 \quad (27)$$

$$\beta_C = \frac{2k_BT}{3\mu}\left(\frac{1}{u^{1/3}} + \frac{1}{v^{1/3}}\right)(u^{1/3} + v^{1/3}). \quad (28)$$

In the above, ρ_p refers to the intrinsic particle density, taken here to be 2000 kg/m^3. For coagulation without radiative effects (i.e., $Z = 1$), Eq. (26) predicts coagulation rates in the transition regime that are in close agreement with the Fuchs interpolation formula (Fuchs, 1989) and other theoretically-based kernels (Sitarski and Seinfeld, 1977; Sceats, 1986).

Two different analytical techniques were used to approximate the solution to Eq. (25) for radiative equilibrium thermophoretic coagulation. The first technique made use of the computationally-simple method-of-moments approximation (Cohen and Vaughan, 1971; Rosner and Tassopoulos, 1991). To utilize this method, we assume that the PSD function retains a log-normal form as given by Eq. (23), with radius a replaced by $(3v/4\pi)^{1/3}$. The kth moment of the number density distribution can then be expressed in a closed-form by

$$\mu_k = \int_0^\infty v^k n(v)\,dv = N_p v_g^k \exp\left(\frac{k^2}{2}\ln^2\sigma_g\right). \quad (29)$$

Note that $\mu_0 = N_p$ and $\mu_1 = \phi$.

Taking the particle volume fraction ϕ to be constant, Eq. (25) is reduced using the method-of-moments to a closed set of three ordinary differential equations, given by (Cohen and Vaughan, 1971)

$$\frac{d\mu_0}{dt} = -\frac{1}{2}\int_0^\infty\int_0^\infty \beta(u,v)n(u)n(v)\,du\,dv \quad (30)$$

$$\frac{d\mu_1}{dt} = 0 \quad (31)$$

$$\frac{d\mu_2}{dt} = \int_0^\infty\int_0^\infty \beta(u,v)n(u)n(v)uv\,du\,dv. \quad (32)$$

The imposition of a constant ϕ requires that the gas temperature T_g remain fixed. To satisfy the radiative equilibrium condition in Eq. (22) for a fixed gas temperature, the incident radiation G is allowed to vary as the PSD evolves.

The problem is nondimensionalized by defining the dimensionless time and number density as,

$$\tau \equiv \frac{2k_BT_gN_{p,0}}{3\mu}t, \qquad \bar{N}_p \equiv \frac{N_p}{N_{p,0}}. \quad (33)$$

Although the method-of-moments results in a relatively compact and numerically efficient approximation to the GDE, a considerable computational overhead is involved in integration of the equations for radiative equilibrium thermophoretic coagulation. At each time step the radiative equilibrium condition in Eq. (22) was solved for the incident radiation G as a function of the fixed gas temperature T_g and the current values of v_g and σ_g. In general, this would require a double integration over particle volume and radiation wavelength, although in practice integration over wavelength at each step was avoided by spline fitting $\bar{C}_e$ as a function of particle size for the given T_g at the beginning of the calculations. Splines were also used to evaluate $\bar{C}_a$ for the given incident wavelength. Once G was obtained at the particular time step, the coagulation factor Z and coagulation rate β were obtained from Eqs. (11) and (26) and used in the double integrals over particle volume in Eqs. (30) and (32). Integration over time was performed using a Runge-Kutta scheme integration with adaptive stepsize (Press et al., 1986), and Gaussian quadrature was used to evaluate the integrals over particle volume.

Results of the numerical computation are given in Figures 4 and 5. As before, two incident wavelengths 10.2 and 0.5145 μm were used, and the gas temperature was 600 K. The initial PSD parameters in both cases were $a_g = 0.1$ μm and $\sigma_g = 2.2$. The initial value of σ_g corresponds closely to the log-normal approximation of the self-preserving size distribution function for continuum Brownian coagulation (Lee, 1983). Consequently, in the absence of

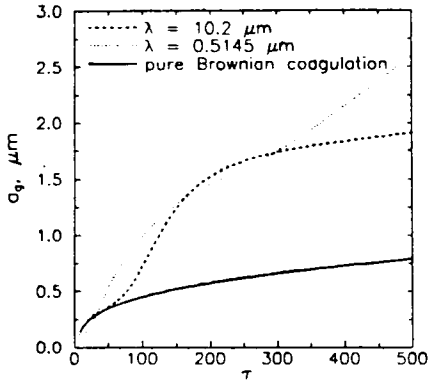

FIGURE 4. Method-of-moments results: geometric mean diameter evolution.

thermophoretic effects, σ_g would remain essentially constant.

Plotted in Figure 4 is a_g versus τ for the two different cases of incident radiation, along with results corresponding to pure Brownian coagulation (i.e., $Z = 1$) for the same conditions. For both incident wavelengths, radiation-induced coagulation is seen to result in a fast initial growth of particle size with respect to Brownian coagulation. Once the mean radius a_g becomes around 1.5 μm, however, the two wavelength cases show a marked difference. Because of the "inversion" in the emission-absorption distribution, large particles under long-wavelength illumination become heated, which results in the observed tapering off of the growth rate. The inversion does not occur for the short wavelength incident radiation, and the growth rate continues to increase in magnitude.

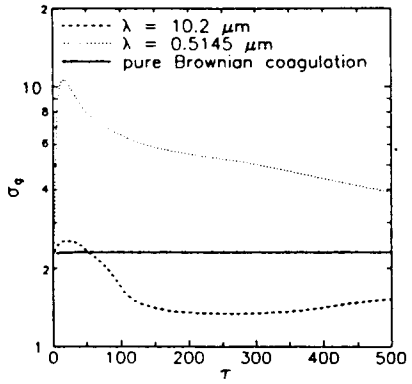

FIGURE 5. Method-of-moments results: σ_g evolution.

The real differences between the two radiation cases, however, are found in the σ_g results. Plotted in Figure 5 is σ_g versus τ for the 10.2 and 0.5145 μm radiation along with the Brownian coagulation values. As expected, the 10.2 μm PSD evolution undergoes an initial broadening, followed by a rapid narrowing of the distribution. Short wavelength radiation, on the other hand, results in an unrealistically wide ($\sigma_g \approx 10$) distribution within a relatively short time. The width of the distribution decreases somewhat for greater times, yet remains at a value considerably higher than that attained for the self-preserving PSD. To give an idea of the dimensional times involved in the calculations, for the given initial a_g and σ_g and a volume fraction of 10^{-6}, the characteristic coagulation time $t_c = 3\mu/2N_{p,0}k_BT_g$ is around 20 sec—so a dimensionless time of $\tau = 200$, for which the 10.2 μm PSD is narrowest, would be attained on the order of 10 sec.

The accuracy of the method-of-moments technique may be questionable for the highly size-dependent coagulation rates β occurring under thermophoretic coagulation—especially in cases in which the PSD width, as reflected in σ_g, is predicted to become very large as in Figure 5. Indeed, qualitative interpretations of PSD evolution would suggest that, for accelerated large particle growth, the actual distribution could become bimodal and would thus have little in common with the monomodal log-normal distribution.

Consequently, PSD evolution under radiative equilibrium thermophoretic coagulation was also investigated using a discretized (or sectional) formulation of the GDE. The numerical method adopted here used the computationally efficient formulation developed by Hounslow et al. (1988). Basically, the number density N_p is divided into "bins," each corresponding to a particular particle volume, that is,

$$N_p = N_0(v_0) + N_1(v_1) + \cdots + N_M(v_M). \tag{34}$$

In an exact representation, the volume domain would be discretized such that $v_1 = 2v_0$, $v_2 = 3v_0$, and so on. Although this approach guarantees that total particle volume will be conserved, it is typically not feasible in view of the considerable number of equations that are needed to represent even a relatively narrow size distribution.

To alleviate this problem, Hounslow et al., chose a geometric volume discretization in which $v_i = 2v_{i-1}$. An advantage of this subdivision is that, to form a particle of the ith size through coagulation of two smaller particles, at least one of the two particles must be in the $i-1$ size. However, conservation of particle volume is no longer automatically satisfied. The formulation of the GDE for this discretization was therefore "weighted" in such a way that the total particle volume would be identically conserved in the specific case of constant β. Without going into the details behind the derivation, the discretized equations for N_i, $i = 0, 1, 2, \ldots, M$, are written,

$$\frac{dN_i}{dt} = N_{i-1}\sum_{j=1}^{i-2} 2^{j-i+1}\beta_{i-1,j}N_j + \tfrac{1}{2}\beta_{i-1,i-1}N_{i-1}^2 - N_i\left[\sum_{j=1}^{i-1} 2^{j-i}\beta_{i,j}N_j - \sum_{j=i}^{M}\beta_{j,i}N_j\right]. \tag{35}$$

Under the discretized PSD approximation, the radiative equilibrium condition in Eq. (22) is expressed as a finite sum, that is,

$$\sum_{i=0}^{M}\left[G\bar{C}_a(a_i) - 4\pi\sigma T_g^4\bar{C}_e(a_i, T_g)\right]N_i = 0. \tag{36}$$

Aside from the above modification, the expressions for radiative properties and coagulation rates were identical to those used in the moment method calculations, and the same Runge-Kutta scheme was employed to integrate the equations for N_i over time. In the results presented below, the gas temperature was again fixed at 600 K, and the PSD evolution under 10.2 and 0.5145 μm monochromatic incident radiation was calculated. For these calculations, however, the initial PSD condition consisted of a monodispersion of 0.1 μm radius particles.

The results of the discretized PSD calculations support the previous conclusions—in that incident radiation wavelength plays a profound role in shaping the PSD spectrum. Presented in Figures 6 and 7 are plots of dimensionless number density $\bar{N}_i = N_i/N_p$ versus particle radius a for the two incident radiation wavelengths and for several values of dimensionless time τ. In Figures 8 and 9 the dimensionless volume fractions $\bar{\phi}_i = N_i v_i/\phi$ are presented for the same conditions. The 10.2 μm results (Figure 6) reveals the "focussing" nature of the coagulation process for the long incident wavelength—in that the particles tend to "pile up" in a relatively small number of $\bar{N}_i$ bins corresponding to $a = 1$–3 μm. The nearly monodisperse nature of the distribution attained for $\tau > 100$ is also reflected in the volume (or, equivalently, mass) fraction results in Figure 8.

The $\bar{N}$ results for the 0.5145 μm case (Figure 7), at first glance, suggest that the width of the size distribution is not radi-

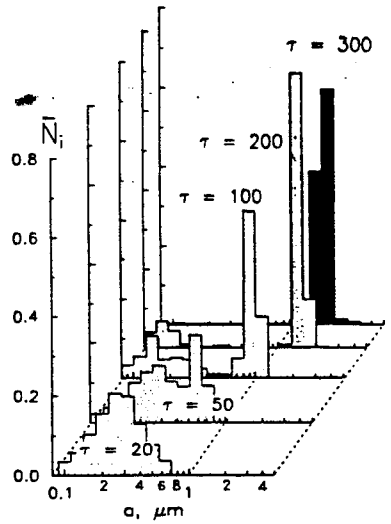

FIGURE 6. Discretized number density results: 10.2 μm radiation.

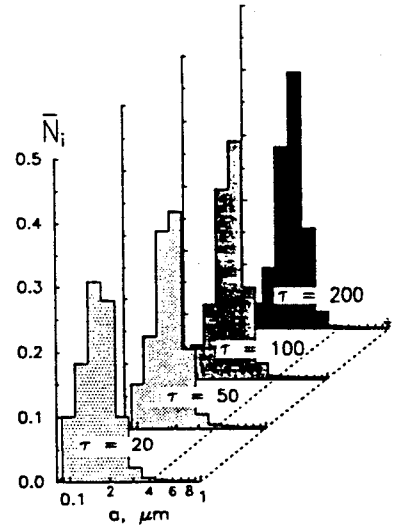

FIGURE 7. Discretized number density results: 0.5145 μm radiation.

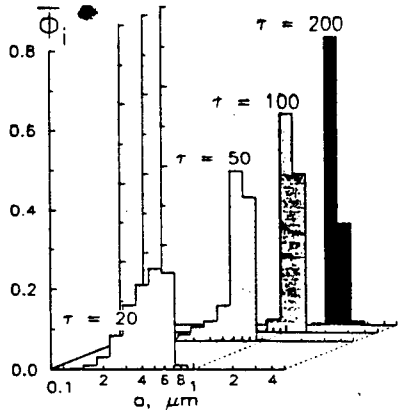

FIGURE 8. Discretized volume fraction results: 10.2 μm radiation.

cally perturbed by the short-wavelength incident radiation. However, since number-averaged mean particle size will always be weighted toward the smaller particle sizes (as opposed to the volume-averaged mean particle size), the results actually indicate that coagulation occurs at a retarded rate among the relatively

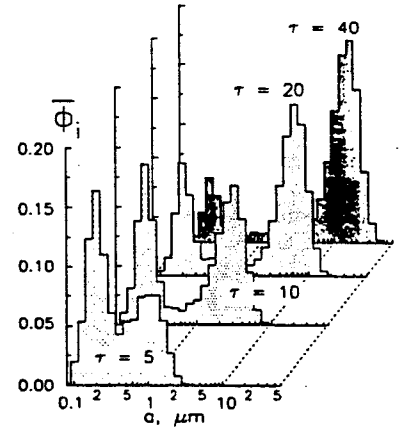

FIGURE 9. Discretized volume fraction results: 0.5145 μm radiation.

small particles in the distribution, as expected. On the other hand, inspection of the volume fraction results in Figure 9 reveals the tremendous growth experienced by the large particles. Note that the time increments in Figure 9 have been reduced to emphasise the "runaway" growth characteristics. As mentioned above, the characteristic coagulation time for initially 0.1 μm particles with a volume fraction of 10^{-6} is about 20 sec. Consequently, the results in Figure 9 indicate that the volume-averaged mean particle size would increase, for the given conditions, by roughly 2 orders of magnitude within 2 sec.

It should be reemphasized that the calculations of PSD evolution under radiative equilibrium are based on several broad simplifications, most significantly a spherical particle assumption. Because of this, the above predictions cannot be taken as quantitative predictions of the behavior of real particles (such as soot aggregates) under the given environmental conditions. However, we would expect the general trends of our predictions, especially with regard to the broadening or narrowing of the PSD spectrum, to remain basically unaffected by a more accurate representation of the coagulation rate constant β. The most important factor in determining whether the PSD broadens or narrows in time is the distribution of radiative heating/cooling among the particle sizes. Regardless of the rate constants, the situation in which the larger and smaller particles are heated and cooled, respectively, would result in the accelerated coagulation of the smaller particles and would thus lead to a narrowing of the particle size distribution. For a given incident radiation wavelength and gas temperature, the emission/absorption balance of a particle depends on the particle emission and absorption cross sections, which, in turn, are primarily a function of particle volume—regardless of particle shape. Consequently, our numerical calculations of PSD evolution, which are formulated in terms of the particle volume, should reasonably account for the effect of increasing particle size on the radiative emission/absorption balance.

The predictions given above are of significance with regard to the "natural" PSD evolution in high-temperature environments, as well as the potential manipulation of particle size and size distribution through external radiation. Although extensive studies involving external radiation other than the long and short monochromatic sources used above have not yet been performed, preliminary calculations indicate that a critical parameter in deciding the fate of the PSD evolution is the ratio of characteristic wavelengths of the incident and emitted radiation. The emission characteristic wavelength will always be on the order of $2898/T_g$ μm, yet the incident wavelength is open to considerable latitude. When the wavelength ratio is less than unity, the PSD tends to broaden in time—as was seen with the 0.5145 μm results. A ratio exceeding 1, however, tends to result in the narrowing of the PSD.

With regard to "natural" conditions, in which the incident radiation would be thermal in nature, it appears that only the former, diverging situation would exist. Because a blackbody is the perfect radiator, it follows that a particle cloud at a temperature T_g could not be in radiative equilibrium with a source of thermal radiation originating from a temperature lower than T_g. The opposite can certainly occur—in that the particle cloud can be in equilibrium with thermal radiation originating from a temperature exceeding T_g, providing the radiation source has an 'emittance' less than unity and/or a solid angle less than 4π. Consequently, the characteristic wavelength ratio for incident thermal radiation will always be less than unity.

Incident radiation sources, however, do not have to be thermal in nature. High-intensity long-wavelength radiation, provided by laser (or, potentially, microwave) sources could potentially be exploited to narrow particle size distribution through thermophoretic coagulation which would be of considerable benefit to technologies involved in production of materials (pigments, catalysts) in small-particle form. Of course, a considerable amount of theoretical and experimental work remains to be performed before the engineering potential of radiation-altered coagulation can be ascertained.

6. CONCLUSIONS

The intention of this work has been to explore previously neglected consequences of radiation heat transfer on the coagulation dynamics of small particles. Although the theoretical analysis has relied on a considerable degree of simplification, the results certainly suggest that radiation-driven particle coagulation and transport mechanisms could play a significant role in particle growth rate and in shaping the particle size distribution.

In high-temperature combustion environments, "natural" radiative emission from near-μm-sized particles could lead to large particle formation. On the microscopic level, radiative emission from individual particles can act to increase the collision rates with neighboring particles. The removal of thermal energy from the gas via particle radiation will also perturb the gas temperature field on the macroscopic level. The effects of the energy removal on the particle dynamics will depend greatly on the initial and boundary condition of the macroscopic system. Under certain conditions, the energy removal could, through particle "compression," significantly accelerate the microscopic level effects.

A specific situation in which the macroscopic-level effects disappear is the condition of radiative equilibrium. In this state, the net macroscopic-level energy transfer to the gas is zero. However, for incident radiation sources having spectra different than that of a blackbody, we show that the individual particles can experience a nonzero net transfer of radiant energy, with some particles absorbing more than they emit and others emitting more than they absorb. The microscopic-level thermophoretic coagulation mechanism will then act to increase the coagulation rates of certain particle sizes, and decrease the coagulation rates of other sizes. Depending on the nature of the incident radiation and the optical characteristics of the particles, coagulation occurring in radiative equilibrium conditions could actually lead to a narrowing of the PSD function.

The work presented here was begun while DWM was a postdoctoral research associate at the High Temperature Chemical Reaction Engineering Laboratory, Chemical Engineering Department, of Yale University. The authors have benefitted from helpful discussions with A. G. Konstandopoulos and M. Vedha-Nayagam.

REFERENCES

Bohren, C. F., and Huffman, D. R. (1983). *Absorption and Scattering of Light by Small Particles*, Wiley, New York.

Cohen, E. R., and Vaughn, E. U. (1971). *J. Coll. Interface Sci.* 35:612–623.

Drolen, B. L., and Tien, C. L. (1986). *J. Quant. Spect. Rad. Transfer* 37:433–448.

Eisner, A. D., and Rosner, D. E. (1985). *Combust. Flame* 61:153–166.

Friedlander, S. K. (1977). *Smoke, Dust and Haze*, John Wiley, New York.

Friedlander, S. K., and Wang, C. S. (1966). *J. Coll. Interface Sci.* 24:170–179.

Fuchs, N. A. (1989). *Mechanics of Aerosols*, Dover Press, New York.

Hampl, V., Kerker, M., Cooke, D. D., and Matijevic, E. (1971). *J. Atmos. Sci.* 28:1211–1221.

Hounslow, M. J., Ryall, R. L., and Marshall, V. R. (1988). *AIChE J.* 34:1821–1832.

Lee, K. W. (1983) *J. Coll. Interface Sci.* 92:315–325.

Lee, S. C., and Tien, C. L. (1981). *Eighteenth Symposium (International) on Combustion*. The Combustion Institute, Pittsburgh, PA, p. 1159.

Loyalka, S. K., and Cipolla, J. W. (1971). *Phys. Fluids* 14:1656–1661.

Mackowski, D. W. (1990). *J. Coll. Interface Sci.* 140:138–157.

Megaridis, C. M., and Dobbins, R. A. (1989). *Twenty-Second Symposium (International) on Combustion*. The Combustion Institute, Pittsburgh, PA, p. 353.

Press, W. H., Flannery, B. P., Teukolsky, S. A., and Vetterling, W. T. (1986). *Numerical Recipes*. Cambridge University Press, Cambridge.

Rosner, D. E. (1986). *Transport Processes in Chemically Reacting Flow Systems*, Butterworths, Stoneham, MA, p. 465.

Rosner, D. E., Mackowski, D. W., Tassopoulos, M., Castillo, J., and Garcia-Ybarra, P. (1992). *Ind. Eng. Chem. Res.* 31:760–769.

Rosner, D. E., and Tassopoulos, M. (1991). *J. Aerosol Sci.* 22:843–867.

Santoro, R. J., Semerjian, H. G., and Dobbins, R. A. (1983). *Comb. Flame* 51:203–218.

Sceats, M. G. (1986). *J. Chem. Phys.* 84:5206–5208.

Sitarski, M., and Seinfeld, J. H. (1977). *J. Coll. Interface Sci.* 61:261–271.

Slinn, W. G. N., and Hales, J. M. (1971). *J. Atmos. Sci.* 28:1465–1471.

Smoluchowski, M. V. (1917). *Z. Physik. Chem.* 92:129.

Sparrow, E. M., and Cess, R. D. (1978). *Radiation Heat Transfer*, McGraw-Hill, New York.

Talbot, L., Cheng, R. K., Schefer, R. W., and Willis, D. R. (1980). *J. Fluid Mech.* 101:737–758.

Tsang, T. H., and Rao, A. (1988). *Aerosol Sci. Tech.* 9:271–277.

Vedha-Nayagam, M., and Mackowski, D. W. (1992). Radiation-induced thermophoretic effects on particle concentration in laminar tube flow, Western States Section/The Combustion Institute Fall Meeting, Berkeley, CA, paper no. 92–114.

Viskanta, R., and Menguç, M. P. (1987). *Prog. Energy Combust. Sci.* 13:97–160.

Wang, H. C., Leong, K. H., Stukel, J. J., and Hopke, P. K. (1983). *Atmos. Envir.* 17:2533–2537.

Zebel, G. (1966). *Aerosol Science*, C. N. Davies, Ed., Academic Press, New York, p. 31.

Received June 21, 1993; accepted July 28, 1993.

See, also;

760 Reprinted from I&EC RESEARCH, 1992, 31.

Effects of Heat Transfer on the Dynamics and Transport of Small Particles Suspended in Gases

Daniel E. Rosner,* Daniel W. Mackowski,† Menelaos Tassopoulos, Jose Castillo,‡ and Pedro Garcia-Ybarra‡

Chemical Engineering Department, High Temperature Chemical Reaction Engineering Laboratory, Yale University, New Haven, Connecticut 06520-2159

Heat transfer (associated with Fourier diffusion, photon absorption and/or emission, surface chemical reaction, and/or evaporation) can lead to dramatic changes in the motion of small particles in gases, modifying coagulation rates, and/or capture rates. Cases discussed in this review of recent studies include (a) *thermophoretic* drift of spherical particles in a gas through which energy is diffusing, (b) *photophoretic* drift of radiation-absorbing suspended spheres, (c) phoresis and apparent Brownian diffusivity of *asymmetric* particles, including spheres with nonuniform accommodation coefficient and unequal primary particle size aggregates, (d) scavenging of fine particles by evaporating droplets, and (e) coagulation rate of unequal temperature spherical particles. These transport phenomena, often associated with the localized "overheating" or "undercooling" of individual particles, have largely been ignored by applied scientists on the (usually implicit) assumption that the more familiar effects of ordinary Brownian diffusion would dominate in near-isothermal laminar gas (sub-)regions. However, we show that even in regions free of macroscopic (bulk) temperature gradients, these phenomena can dominate ordinary Brownian transport by orders of magnitude, with potentially important engineering consequences. General expressions for the relevant particle drift velocities, coagulation rate constants, or effective particle diffusivities are used to carry out illustrative calculations for multiphase systems of current and future engineering interest, including fine particle synthesis/materials processing, and combustion gas cleaning.

REPORT DOCUMENTATION PAGE

Form Approved
OMB No. 0704-0188

1. AGENCY USE ONLY (Leave blank)	2. REPORT DATE	3. REPORT TYPE AND DATES COVERED
	1993	CONF. PROC. (BOOK, Paper)

4. TITLE AND SUBTITLE

ONSET CONDITIONS FOR GAS PHASE REACTIONS AND PARTICLE NUCLEATION/GROWTH IN CVD BOUNDARY LAYERS.

5. FUNDING NUMBERS

PE - 61102F
PR - 2308
SA - BS
G - 91-0170(AFOSR)

6. AUTHOR(S)

D.E. Rosner , J. Collins and J.L. Castillo

7. PERFORMING ORGANIZATION NAME(S) AND ADDRESS(ES)

HIGH TEMPERATURE CHEMICAL REACTION ENGINEERING LABORATORY
YALE UNIVERSITY
BOX YALE STATION
NEW HAVEN, CONNECTICUT 06520 U.S.A.

8. PERFORMING ORGANIZATION REPORT NUMBER

9. SPONSORING/MONITORING AGENCY NAME(S) AND ADDRESS(ES)

AFOSR/NA
Building 410
Bolling AFB DC 20332-6448

10. SPONSORING/MONITORING AGENCY REPORT NUMBER

11. SUPPLEMENTARY NOTES

12a. DISTRIBUTION/AVAILABILITY STATEMENT

Approved for public release; distribution is unlimited

12b. DISTRIBUTION CODE

13. ABSTRACT (Maximum 200 words)

Literature CVD-rate data, and our recent experiments on TiO_2(s) film growth from titanium (IV) tetra-isopropoxide (TTIP) vapor using a well-defined impinging jet reactor, reveal that the onset of vapor phase reactions near a hot deposition surface can lead to sharp reductions in CVD-rate and alterations in deposit microstructure. These observations have motivated our development of a thin *chemical sublayer* (CSL-) theory for predicting (using simple formulae) the interplay of *heterogeneous* kinetics, *homogeneous* kinetics and (Fick-, Soret-, convective-) *transport* phenomena in CVD reactors. CSL theory, only briefly outlined here, can be used to interrelate different CVD reactors/conditions and thereby guide the selection of reactor configurations/conditions that will lead to the maximum CVD-rate prior to the onset of vapor phase reactions and/or external transport limitations. Comparisons with our present TiO_2(s) (*via* TTIP) data are used to suggest fruitful extensions of this work.

14. SUBJECT TERMS

chemically reacting sublayer (CSL-) theory , TiO_2 CVD rate data

15. NUMBER OF PAGES

7

16. PRICE CODE

17. SECURITY CLASSIFICATION OF REPORT	18. SECURITY CLASSIFICATION OF THIS PAGE	19. SECURITY CLASSIFICATION OF ABSTRACT	20. LIMITATION OF ABSTRACT
Unclassified	Unclassified	Unclassified	UL

12 th International Conference on CVD
Electrochemical Soc., Hawaii, May 15-21, 1993
Proc. Vol. 93-2

ONSET CONDITIONS FOR GAS PHASE REACTIONS AND PARTICLE NUCLEATION/GROWTH IN CVD BOUNDARY LAYERS.

D.E. Rosner[a], J. Collins[b] and J.L. Castillo[c]
High Temperature Chemical Reaction Engineering Laboratory
Yale University, Department of Chemical Engineering
New Haven CT 06520-2159, USA

Literature CVD-rate data, and our recent experiments on TiO_2(s) film growth from titanium (IV) tetra-isopropoxide (TTIP) vapor using a well-defined impinging jet reactor, reveal that the onset of vapor phase reactions near a hot deposition surface can lead to sharp reductions in CVD-rate and alterations in deposit microstructure. These observations have motivated our development of a thin *chemical sublayer* (CSL-) theory for predicting (using simple formulae) the interplay of *heterogeneous* kinetics, *homogeneous* kinetics and (Fick-, Soret-, convective-) *transport* phenomena in CVD reactors. CSL theory, only briefly outlined here, can be used to interrelate different CVD reactors/conditions and thereby guide the selection of reactor configurations/conditions that will lead to the maximum CVD-rate prior to the onset of vapor phase reactions and/or external transport limitations. Comparisons with our present TiO_2(s) (*via* TTIP) data are used to suggest fruitful extensions of this work.

1. INTRODUCTION

To interpret our recent experimental observations on the CVD rate of TiO_2 films in an impinging jet reactor (1,5) and guide the design/operation of future CVD reactors, a rational asymptotic theory has been developed for the onset of homogeneous chemical reactions in the thermal boundary layer (BL) adjacent to a hot deposition surface, with emphasis on their effect on deposition rates and film quality (1,2). The analysis is tailored to systems in which a) gas phase reactions are confined to a thin *chemical sublayer* (CSL) embedded inside the thermal BL and b) the homogeneous reaction(s) of interest can be represented by a single high activation energy ($E_{hom}/(RT_e) >> 1$) Arrhenius-type rate expression. In this limit one finds (2):

---

[a] Professor of Chemical Engineering and Director, HTCRE Laboratory HTCRE Ms. #195
[b] Graduate Research Assistant, Yale HTCRE Laboratory
[c] Visiting Scholar; Permanent Address: U.N.E.D., Dept. Physics, Madrid 28080, Spain

$$\frac{\delta_{CSL}}{\delta_h} \approx \left(\frac{E_{hom}}{RT_e}\right)^{-1} \cdot \frac{\theta_w^2}{\theta_w - 1} \qquad [1]$$

where θ_w ($\equiv T_w/T_e$) is the temperature ratio across the thermal BL of slope thickness δ_h. Because of the large molecular weight disparities and high temperature gradients prevailing in many CVD systems (3,4), we allow for the Soret reduction of dilute reagent Fick transport to the hot surface. The resulting closed-form expressions provide CVD-rate predictions and rational quantitative criteria for "vapor phase ignition" (VPI) in terms of CVD system parameters and the "known" chemical kinetic parameters characterizing the vapor reactants. Conversely, armed with such a theory, one can use experimentally observed VPI conditions to infer the effective homogeneous kinetic parameters for the system in question—information often not independently available. In effect, we are recommending use of the gaseous boundary layer itself as a "flow reactor", with the CVD surface acting as a detector of the "remaining reactant." Our general results can be easily applied to specific ceramic film systems of current interest, with our present emphasis being the CVD of TiO_2(s) (from $TiCl_4$ or TTIP+ O_2)

The overall trends predicted by CSL theory are displayed in Fig. 1 over a broad range of heterogeneous Damkohler numbers Dam_{het} ($\equiv A_{het}\,\delta/D$)-values and T_e/T_w-values, for particular dimensionless activation energies $E_{hom}/(RT_e)$ and $E_{het}/(RT_e)$, homogeneous Damkohler number Dam_{hom} ($\equiv A_{hom}\,\delta^2/D$) and Soret factor α_T (2,3). Here A_{het} and A_{hom} are, respectively, the heterogeneous and homogeneous rate constant *pre-exponential* factors. In the CVD reactor described below(1,5) using $TiCl_4$(g) as the Ti-carrier we were unable to study such VPI trends at convenient surface temperatures, however, the use of TTIP provided what appears to be a clear cut example of this phenomenon (see Fig. 3 below). From available estimates of the overall *homo*geneous chemical kinetics of this system, we infer $E_{hom}/(RT_e) \approx 22$ and $\theta_w \approx 3$, which implies (Eq.[1]) that $\delta_{CSL}/\delta_h \approx 1/5$. This thickness ratio *may* be small enough to apply chemical sublayer theory as a useful first approximation, but because of its magnitude we have also initiated a finite-element numerical attack on this same example (8), as well as needed generalizations of CSL-theory. Incidentally, an interesting previously observed example of VPI using $TiCl_4$(g) (6) could not be analyzed using our present approach due to uncertain (undocumented) transport conditions .

2. EXPERIMENTAL

We are now investigating "vapor phase ignition" (VPI) under well-defined transport conditions using an axisymmetric impinging laminar jet "pedestal" CVD reactor (Fig. 2). Upon entering the reactor, cold (300-400 K)

reagent vapor ($TiCl_4$ or TTIP) and carrier gas (Ar or N_2) flow through a short mixing chamber and a converging nozzle. The laminar jet emerging from the nozzle impinges on a polished quartz substrate ($d_{substrate} = d_{jet} = 12.7mm$; located roughly one jet diameter downstream) heated from below by an RF-heated graphite susceptor . CVD-rate measurements are by *in situ* interferometry (at 633 nm) and/or *ex situ* weight gain. Deposit microstructures are studied using scanning electron microscopy (SEM).

Preliminary experiments were for titania deposition from $TiCl_4/O_2/Ar$ and $TiCl_4/N_2O/Ar$ at 0.1 MPa total pressure(1). To explore VPI phenomena at more accessible substrate temperatures, we shifted to titanium(IV)-iso-propoxide ($Ti(OC_3H_7)_4$) in N_2 with a small amount of added oxygen to "burn away" any co-deposited carbon. The liquid reagent source is a constant temperature bubbler. All reagent lines are teflon or stainless steel, heated above the reagent vapor dew point. To avoid water contamination the reactor is pumped down to 10 Pa for several hours before each run and only ultra high purity Ar and N_2 gases are used ($[H_2O] < 0.5$ ppm).

Our current range of accessible operating conditions (with well-defined fluid flow) are: substrate temperature T_w up to 1600 K, total pressure p between 0.01 and 0.1 MPa, and impinging jet Reynolds number, Re_{jet}, between roughly 200 and 800 (based on nozzle diameter, d_{jet}). Under these conditions natural convection is not expected in the jet impingement region since $Re_{jet}^{1/2}/Gr_h^{1/4} >> 1$, ($Gr_h$ is the heat transfer Grashof number for the impinging jet boundary layer (see, *e.g.*,(9))). Moreover, we estimate negligible entrainment of recirculating reaction products in the impingement region.

3. RESULTS

As shown in Fig. 3, in the CVD of TiO_2 from TTIP above $T_w \approx 1150K$ we have observed a deposition rate fall-off to about 1/10th of the diffusion-controlled plateau value. In Fig 3, k_{eff} is an effective first order rate constant defined as the absolute molar deposition flux $(-j_w"/M)_{TTIP}$ divided by a reference concentration $[P_{TTIP,e}/(RT_w)]$. The apparent activation energy of the *heterogeneous* kinetics controlled region below 750 K is about 132 KJ/mole. Before reaching VPI, our data go through a broad diffusion-controlled plateau. The actual rate fall-off region above *ca.* 1150K shows a slope of roughly -70 KJ/mole. The break-point temperature may be influenced by reagent concentration, total pressure and flow rate, and we are currently investigating these possibilities. Preliminary analysis of SEM micrographs of TiO_2 deposits from TTIP shows that relatively smooth, dense polycrystalline films are produced under heterogeneous kinetics-controlled conditions ($T_w <$ 750K). Under diffusion-controlled conditions we observe massive (*ca.* 40μm) and poorly adherent dendritic structures. Interestingly, films produced well

above the onset of VPI show higher density and improved substrate adherence.

4. DISCUSSION

Using CSL-theory(2) we can readily predict the wall concentration and deposition flux of reagent, allowing for depletion due to CSL reactions. In cases where the homogeneous reactions generate non-depositing products, this 'surviving' reagent deposition flux should equal the experimentally observed deposition rate. The closed form asymptotic theory yields all expected transitions in deposition regimes for CVD systems in which $E_{hom} > E_{het}$ (*cf.* Fig. 1). At sufficiently low surface temperatures the *homo*geneous reaction is suppressed and the CVD-rate is limited by the intrinsic *hetero*geneous chemical kinetics. However, as T_w increases, gas phase transport limitations set in (see below) and TTIP vapor reactions become increasingly important, ultimately causing the deposition flux of virgin reagent to *decrease* (Figs.1,3). In the present ($TTIP/O_2$) system, this occurred after the broad external diffusion-controlled plateau ($750 < T_w < 1150K$) revealed in Fig.3.

To within our experimental errors (±10%) the 'plateau'-value of k_{eff} is seen to correspond to our estimate of $\delta_{h,eff}$ based on earlier impinging laminar jet heat transfer measurements, provided a significant correction is made for the Soret-reduction(3,4) in diffusion-controlled TTIP mass transfer rate (*ca.* ⅓ at VPI, based on an estimated α_T-value of 1.6) and systematic corrections for non-constant properties (*ca.* 15%) and nonunity Lewis number (*ca.* 33%, since $D_{TTIP-N2}/(k/(\rho c_p)) \approx 0.26$). No appreciable Stefan flow ("suction") correction was necessary (see, eg.,(10)) since, in these experiments the mass fraction of TTIP in the feed was only 0.5%, corresponding to a titanium *element* mass fraction(9) of only 0.08%. Indeed, the present version of CSL theory(2) also neglects Stefan flow phenomena, as is appropriate in the 'dilute' reagent limit.

For a first order homogeneous reaction CSL-theory predicts that VPI should occur approximately where:

$$\theta_{w,VPI} = (E_{hom}/(RT_e)) \bullet \{ \ln[Dam_{hom} \bullet (E_{hom}/(RT_e))^{-1}]\}^{-1} \qquad [2]$$

when VPI occurs along the diffusion-controlled branch (Figs.1,3). The experimentally observed value, $\theta_{w,VPI} \approx 1150/380 = 3.0$, is in approximate accord with published values(11) of E_{hom} (70.5 KJ/mole) and $A_{hom}(4x10^5\ s^{-1})$, since, under our experimental CVD conditions we expect $Dam_{hom} \approx O(10^4)$. While CSL theory(2) also predicts that the ultimate slope of the fall-off region should correspond to an apparent activation energy of $-(E_{hom} - E_{het})$, the observed slope appears closer to $-E_{hom}$. This may indicate that at such high

surface temperatures E_{het} has decreased to values small compared to E_{hom}. Extended CVD-rate data and future generalizations of CSL-theory should clarify this situation, and provide further valuable tests of CSL theory.

Returning to the onset of appreciable external diffusion limitations, for a first order heterogeneous reaction this should occur at the T_w-value for which $Dam_{het} \cdot \exp[- E_{het}/(RT_w)] \approx 1$. This point, also shown on Fig.3, is consistent with our own lower temperature (A_{het}, E_{het}-)data. In considering the two "end-points" shown on Fig. 3, we remark that in many situations merging them, if acheivable, would be an optimum operating point. This would maximize chemically-controlled CVD-rates while just avoiding increased sensitivity to position and gas-dynamic conditions (leading, also, to surface roughness), as well as avoiding deposit defects associated with the capture/incorporation of embryonic microparticles.

5. CONCLUSIONS and RECOMMENDATIONS

Using TiO_2 CVD rate data (1,5, Fig. 3), we have demonstrated that an asymptotic *chemically reacting sublayer* (CSL-) theory(2) can provide useful estimates of unreacted reagent concentrations and wall fluxes at CVD surfaces. This opens the way to rationally interrelate different CVD reactors environments *via* the intermediary of their global reaction kinetic parameters (2). Simple CSL-theory is applicable and convenient for reactor design/optimization whenever homogeneous reactions can be represented by a global reaction with $E_{hom}/(RT_e) >> 1$ and the temperature ratio across the boundary layer is also sufficiently large (*cf.* Eq. [1]). This approach could also be exploited in computational methods when high activation energies and large local gradients preclude accurate numerical treatment of the actual network of homogeneous chemical reactions. Thus, the structure of such "chemical sublayers" can be computed (using "rescaled" coordinates) in greater chemical detail by exploiting geometrical and property value *simplifications valid because of their thinness.* Indeed, even when conventional boundary layer theory breaks down (due to inadequate $(Re \cdot Pr)^{1/2}$; see, eg, (9)), boundary layer approximations may remain valid and useful for such *chemical sublayers* — as will be demonstrated our follow-on research.

Our current investigations include obtaining direct experimental corroboration of vapor phase reaction onset, generalizing CSL-theory, and developing a self-consistent theory which explicitly accounts for the production, growth and transport of clusters within CVD-boundary layers.

ACKNOWLEDGEMENTS

These flow reactor experiments are supported by AFOSR (Grant 91-0170) at Yale University , HTCRE Laboratory. We thank J. Tsang (Yale ChE '93) for his assistance with our TiO_2 *via* $TiCl_4$ experiments, and J. Setlock (NASA Lewis Laboratories) for his assistance in the SEM-characterization of our TiO_2 films. Our CVD theoretical studies were supported by NASA-Lewis RC under Grants NAG 3-884 and NTG-5037. The authors have benefitted from discussions and ancillary calculations of Dr. S.A. Gökoğlu and G.W. Stewart, NASA-Lewis RC.

6. REFERENCES

1. J. Collins, D.E. Rosner and J.L. Castillo, "Onset Conditions for Gas Phase Reaction and Nucleation in the CVD of Transition Metal Oxides", Mat. Res. Soc. Symp. Proc. **250**, 53 (1992).
2. D.E. Rosner, J.L. Castillo and M. Tassopoulos, "Role of High Activation Energy Homogeneous Reactions in Limiting CVD-Rates and Deposit Quality for Heated Surfaces", Paper no. 55d, 1990 AIChE Meeting (Chicago, IL); J. Electrochem. Soc. (submitted 1993)
3. D.E. Rosner, "Thermal (Soret) Diffusion Effects on Interfacial Mass Transport Rates", J. PhysicoChemical Hydrodynamics, (Pergamon)**1**, 159-185 (1980).
4. D.E. Rosner, "Transport Processes and Chemical Kinetics in High Temperature Lamp Modeling", Proc. Symposium on High Temperature Lamp Chemistry, Electrochemical Soc.Public. **88-4**, 11-138 (1988).
5 J. Collins, PhD Dissertation, Yale University, Department of Chemical Engineering (in preparation, Spring 1993).
6. R.N. Ghoshtagore, J. Electrochem Soc., **117**(4), 529 (1970); *ibid*, **117**(10), 1310 (1970).
7 S.A. Gökoğlu and D.E. Rosner,"Prediction and Rational Correlation of Thermophoretically Reduced Particle Mass Transfer to Hot Surfaces Across Laminar or Turbulent Forced Convection Gas Boundary Layers", Chem. Eng. Commun., **44**, 107 (1986).
8. S.A. Gökoğlu, G.D. Stewart and J. Collins, (in preparation).
9. D.E. Rosner, **Transport Processes in Chemically Reacting Flow Systems**, Butterworth-Heinemann, Stoneham MA; 3d Printing, 1990
10 D.E. Rosner, "Effects of the Stefan-Nusselt Flow on the Apparent Kinetics of Heterogeneous Reactions in Forced Convection Systems", Int. J. Heat Mass Transfer, **9**, 1233-1253 (1966)
11. K. Okuyama *et.al.*, "Particle Generation in a CVD Process with Seed Particles", AIChE J, **36**(3), 409-419 (1990).

Fig. 1: CSL-theory predicted Arrhenius behavior for CVD-rates in the presence (at high surface temperatures) of vapor phase reactions yielding non-depositing products (2); Dependence of nondimensional CVD-rate (log scale) on (reciprocal) surface temperature and heterogeneous reaction Damkohler number $A_{het}\delta/D$, where A_{het} is the pre-exponential factor of the first-order heterogeneous rate constant.

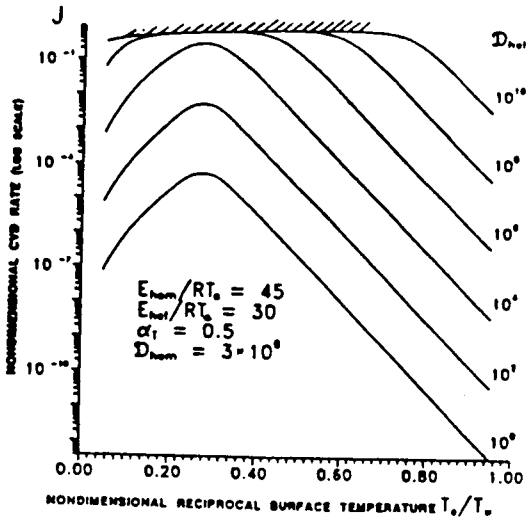

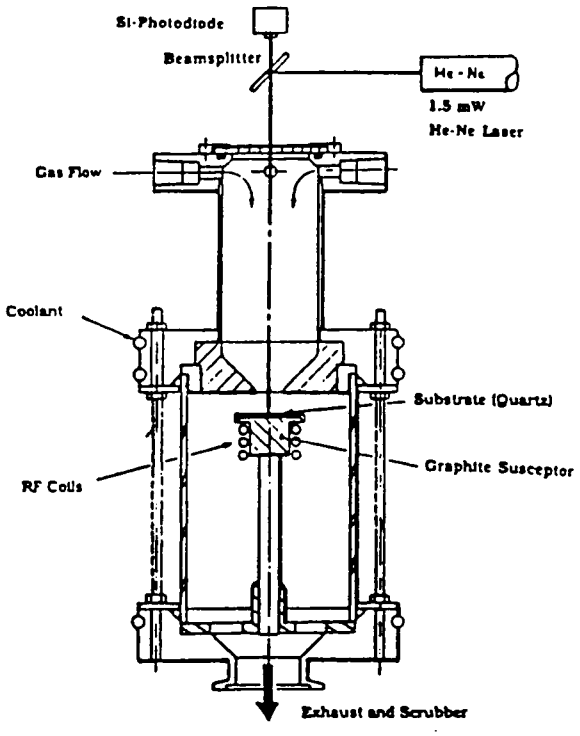

Fig. 2: Axisymmetric impinging jet CVD reactor with inductively-heated "pedestal"; after Collins (1991, 1993)

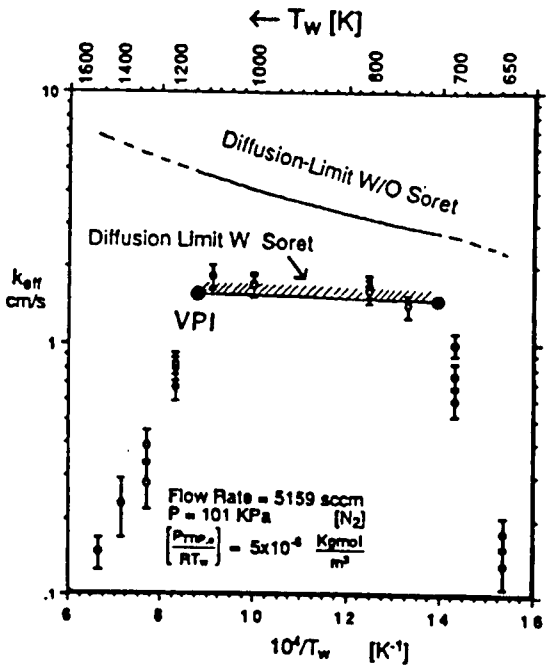

Fig. 3: TiO_2 Deposition rate data from $TTIP/O_2/N_2$ with calculated diffusion-controlled limits showing effect of Soret diffusion

REPORT DOCUMENTATION PAGE

Form Approved
OMB No. 0704-0188

1. AGENCY USE ONLY (Leave blank)	2. REPORT DATE	3. REPORT TYPE AND DATES COVERED
	1993	Reprint: J. Aerosol Sci 24(4) 471-483

4. TITLE AND SUBTITLE

INERTIAL DEPOSITION OF PARTICLES FROM POTENTIAL FLOWS PAST CYLINDER ARRAYS

5. FUNDING NUMBERS

PE - 61102F
PR - 2308
SA - BS
G - 91-0170 (AFOSR)

6. AUTHOR(S)

ATHANASIOS G. KONSTANDOPOULOS, MICHAEL J. LABOWSKY and DANIEL E. ROSNER

7. PERFORMING ORGANIZATION NAME(S) AND ADDRESS(ES)

HIGH TEMPERATURE CHEMICAL REACTION ENGINEERING LABORATORY
YALE UNIVERSITY
BOX 208286 YALE STATION
NEW HAVEN, CONNECTICUT 06520 U.S.A.

8. PERFORMING ORGANIZATION REPORT NUMBER

9. SPONSORING/MONITORING AGENCY NAME(S) AND ADDRESS(ES)

AFOSR/NA
Building 410
Bolling AFB DC 20332-6448

10. SPONSORING/MONITORING AGENCY REPORT NUMBER

11. SUPPLEMENTARY NOTES

12a. DISTRIBUTION/AVAILABILITY STATEMENT

Approved for public release; distribution is unlimited

12b. DISTRIBUTION CODE

13. ABSTRACT (Maximum 200 words)

Abstract—We exploit the computationally efficient method of images (MOI) to create steady potential flows past finite and infinite circular cylinder arrays, in order to study inertial impaction of particles on them. Although such flows are often encountered in practice (e.g. high Reynolds number "dusty gas" flows past heat exchanger tube banks and filter screens), little is yet known about the proximity effects of adjacent collectors on the capture efficiency of any particular collector in the array. Our results for linear, symmetric arrays in steady cross-flow, containing an odd number of collectors (from three to infinity), over a wide range of array spacings, support the conjecture that an appropriately defined *effective Stokes number* based on the stagnation region fluid deceleration rate (computed and reported here as a function of the number of collectors and their spacing) can adequately correlate, for practical purposes, the capture efficiency of a representative collector in the array. This scheme, combined with well-known correlations for an isolated collector, simplifies significantly the task of estimating inertial impaction rates.

14. SUBJECT TERMS	15. NUMBER OF PAGES
inertial impaction, cylinders in crossflow	13
	16. PRICE CODE

17. SECURITY CLASSIFICATION OF REPORT	18. SECURITY CLASSIFICATION OF THIS PAGE	19. SECURITY CLASSIFICATION OF ABSTRACT	20. LIMITATION OF ABSTRACT
Unclassified	Unclassified	Unclassified	UL

J. Aerosol Sci. 24(4)471-483(1993)
Printed in Great Britain.

0021-8502/93 $6.00+0.00

HTCRE #187

INERTIAL DEPOSITION OF PARTICLES FROM POTENTIAL FLOWS PAST CYLINDER ARRAYS*

ATHANASIOS G. KONSTANDOPOULOS,† MICHAEL J. LABOWSKY and DANIEL E. ROSNER

Yale University, Department of Chemical Engineering, High Temperature Chemical Reaction Engineering Laboratory, New Haven, CT 06520-2159, U.S.A.

(*First received* 26 *December* 1991; *and in final form* 26 *October* 1992)

Abstract—We exploit the computationally efficient method of images (MOI) to create steady potential flows past finite and infinite circular cylinder arrays, in order to study inertial impaction of particles on them. Although such flows are often encountered in practice (e.g. high Reynolds number "dusty gas" flows past heat exchanger tube banks and filter screens), little is yet known about the proximity effects of adjacent collectors on the capture efficiency of any particular collector in the array. Our results for linear, symmetric arrays in steady cross-flow, containing an odd number of collectors (from three to infinity), over a wide range of array spacings, support the conjecture that an appropriately defined *effective Stokes number* based on the stagnation region fluid deceleration rate (computed and reported here as a function of the number of collectors and their spacing) can adequately correlate, for practical purposes, the capture efficiency of a representative collector in the array. This scheme, combined with well-known correlations for an isolated collector, simplifies significantly the task of estimating inertial impaction rates.

NOMENCLATURE

d_p particle diameter
$\hat{\mathbf{e}}_x$ x-direction unit vector
$\mathbf{n}^i$ outward unit normal of the ith cylinder
R cylinder radius
S array spacing
Stk Stokes number
t time
$\mathbf{u}$ fluid velocity vector
$\mathbf{u}_p$ particle velocity vector
U_∞ fluid velocity upstream of the collector (at $-\infty$)
x coordinate
y coordinate

Greek letters
μ doublet strength
μ_g dynamic viscosity of gas
ρ_p particle mass concentration (density)
τ particle relaxation time
Φ fluid velocity potential
η_{cap} capture fraction

Subscripts
i impact
sp stagnation point
w at the wall
∞ at infinity

1. INTRODUCTION

Particle inertial behavior results from momentum non-equilibrium between the suspended particles and the host flow and is characterized by the dimensionless Stokes number, Stk (ratio of particle momentum relaxation time, τ to a characteristic flow time-scale, τ_{flow}):

$$\mathrm{Stk} \equiv \frac{\tau}{\tau_{flow}} \tag{1}$$

* Based on Paper 5.E6 presented at the 1990 AAAR Annual Meeting, 18–22 June, Philadelphia, PA, U.S.A.
† Present address: 45 Tselepi Str., Thessaloniki, GR-543 52, Greece.

where (*cf.* Nomenclature):

$$\tau = \frac{\tilde{\rho}_p d_p^2}{18\mu_g} C \tag{2}$$

$$\tau_{flow} = \frac{R}{U_\infty} \tag{3}$$

with $\tilde{\rho}_p$ being the intrinsic particle density, d_p its diameter, μ_g the dynamic viscosity of the carrier gas and C the Stokes–Cunningham slip correction factor accounting for deviations from continuum drag behavior (see, e.g., Friedlander, 1977).

The important role of inertia in transporting large-sized aerosol particles (more specifically particles with Stk-values larger than a critical, flow-field dependent value, Stk_{crit}) to collector surfaces leading to direct impaction has been recognized long ago (see Appendix) and the study of $Stk > Stk_{crit}$ (supercritical) inertial effects is a mature subject in aerosol science (e.g. Fuchs, 1964; Davies, 1966; Friedlander, 1977). Particle deposition rates are usually expressed in terms of the dimensionless *capture fraction*, $\eta_{cap} \in [0, 1]$, defined as the ratio of the actual flow area (at upstream infinity), where depositing particle trajectories originate, over the projected collector area. Too numerous calculations of inertial capture efficiencies exist in the literature for well-known analytically or computationally generated fluid flow fields around isolated collectors to be explicitly mentioned here. A particular geometry, that of an isolated cylinder in cross-flow, has received considerable attention due to its relevance to several practical applications (e.g., filtration by fibrous filters, fouling of heat exchanger tube banks, etc.).

Inertial impaction of particles on an isolated cylinder target, especially at high Reynolds numbers, Re (when potential flow provides a good approximation of the flow field away from the surface of the collector) is now rather well understood. Classic studies in the aerosol literature (for detailed references see Fuchs, 1964; Friedlander, 1977) have been extended to cover large parameter spaces and useful correlations for important quantities of interest have become available for routine engineering predictions. In particular, Israel and Rosner (1983) devised a correlation scheme for the inertial capture efficiency, η_{cap} of isolated cylinders and spheres in steady potential flow, introducing the notion of an "effective Stokes number" Stk_{eff}. Non-linear drag was accounted for,[†] following a suggestion of May and Clifford (1967) to use the actual particle stopping time in the definition of Stk_{eff}. Differences in collector geometry (sphere vs cylinder) were accommodated employing as the characteristic flow time the respective flow deceleration rate at the stagnation point of each collector. It was then possible to "collapse" the characteristic S-shaped, inertial capture efficiency curves for the cylinder and the sphere, in terms of a single, "universal" curve. The scheme was later applied by Wang (1986) in his study of inertial impaction and rebound of particles from cylinders and by Wessel and Righi (1989) who provided extensive correlations, not only for the inertial capture efficiency of a cylinder in potential flow, but also for impact velocities, particle concentrations at the cylinder surface, and angular distributions of quantities of interest. A correlation of numerical results for η_{cap} for inertial impaction from viscous flows ($30 < Re < 40{,}000$) past a single cylinder is given in Ilias and Douglas (1989).

Inertial impaction on collector *assemblies* is less well-studied than the isolated collector cases. Except for some special cases, little is yet known about the "proximity" effects of adjacent collectors on the inertial deposition rates especially from high Re flows on any particular cylinder in an array. This work was motivated by the fact that such situations occur often in practice, e.g. in the entrance region to a heat exchanger tube bank or a fibrous filter screen, as well as in laboratory experiments simulating such arrangements. Neighboring collector effects have been studied more extensively for low Re flows of immediate relevance to filtration processes, either in "unit cell" models (see, e.g., Tien, 1989) or for an infinite array of fibers in cross-flow (e.g., Tsiang *et al.*, 1982; McLaughlin *et al.*, 1986; Ingham

[†] Low transonic flow compressibility effects could also be taken into account using the Stk_{eff} technique (Israel and Rosner, 1983).

et al., 1989). Choudhary and Gentry (1977) apparently were the first to study inertial impaction from steady potential flow on a row of two cylinders, using the method of images (MOI) to construct the inviscid, incompressible flow field. Ingham *et al.* (1989) employed the Boundary Element Method (BEM) to compute the flow field, and focused on the infinite array problem. These authors have also considered, in addition to circular cylinders, elliptical cylinders. Particle trajectories were traced in these flow fields and η_{cap} of a representative collector geometry was evaluated as a function of Stk. Results in both studies were given only for a particular cylinder center-to-center spacing of 5.35 radii. Other more elaborate computations for a cylinder in a "deep" tube bank, using variants of the k_t-ε model of turbulence for the flow field and incorporating particle tracking modules, have also appeared recently (Schuh *et al.*, 1989; Fan *et al.*, 1991) in the interest of predicting tube erosion. Both studies, however, presented only the results of representative numerical calculations but no η_{cap} {Stk, . . .} curves.

In the present work we study inertial impaction on cylinder arrays with the following objectives:

(1) To investigate how the number of collectors and their spacing (⊥ flow) alter the collection characteristics of a single ("test") cylinder in an array.

(2) To find appropriate ways to correlate such data and provide approximate, yet rational methodologies for practical situations that would circumvent the need for further detailed computations of the type that we have performed.

We do not address here the possibility of particle rebound, so that in what follows impaction and capture are treated as synonymous. The structure of the present paper is as follows: In section 2 we outline the numerical calculation of the flow field. In section 3 we provide the results of our particle impaction computations on a representative cylinder in finite and infinite collector arrays. We discuss our correlation scheme for η_{cap} in section 4 and apply it to the data of section 3, while section 5 summarizes the conclusions drawn from this work. An Appendix clarifies some issues concerning the critical Stokes number for particle impaction on bluff bodies.

2. FLOW FIELD COMPUTATION

The inviscid flow field, $\mathbf{u}=-\nabla\Phi$ past an assembly of circular cylinders is determined in terms of the velocity potential Φ, which satisfies Laplace's equation:

$$\nabla^2\Phi=0 \tag{4}$$

subject to the boundary conditions of zero normal velocity on all cylinder walls:

$$\nabla\Phi\cdot\mathbf{n}^i=0 \quad i=1,2,\ldots N_{cyl} \tag{5}$$

and a uniform flow at infinity ($x=-\infty$):

$$-\frac{\partial\Phi}{\partial x}=U_\infty \tag{6}$$

$$\frac{\partial\Phi}{\partial y}=0. \tag{7}$$

Although, in principle, these equations can be solved with a variety of methods, some of the most efficient are those exploiting the superposition of fundamental solutions of Laplace's equation in such a way as to satisfy the boundary conditions (Fletcher, 1988). Superposition (image) methods for the solution of Laplace's equation are well documented in classic fluid mechanics texts (Milne-Thomson, 1955; Lamb, 1932). In what follows we therefore provide only an "algorithmic" sketch of the computational implementation. While our MOI code can handle arbitrary cylinder arrangements of various radii, here we concentrate on the practically important geometry of a straight array of identical cylinders in cross flow. For convenience we have used arrays containing an odd number of cylinders

with the central cylinder, located at the origin serving as our "test" collector. The arrays are characterized by the number of cylinders N_{cyl} and their dimensionless center-to-center spacing, S expressed in cylinder radii units. Potential flow around an isolated cylinder is equivalent to the superposition of a doublet (dipole) singularity (fundamental solution of Laplace's equation in 2-D) at the axis of the cylinder and a uniform stream at infinity:

$$-\Phi = -(\Phi_d + \Phi_\infty) = U_\infty R^2 \frac{x}{x^2+y^2} + U_\infty x. \tag{8}$$

Picking the velocity of the uniform flow at upstream infinity, U_∞, directed along the positive x-axis, as our velocity scale and the cylinder radius R as the length scale the calculation of the dimensionless flow field proceeds as follows:

(1) We first place a doublet at the center of each cylinder in the assembly of unit strength (i.e. normalized with $U_\infty R^2$) aligned with the negative x-axis. We term these the *first generation* doublets.

(2) Using the so-called *image relations* we compute, for each cylinder, the images of all doublets external to the cylinder. The image of a doublet of dimensionless strength μ positioned at a dimensionless distance ℓ from a cylinder center has a dimensionless strength μ/ℓ^2 and is located at the inverse point of the line connecting the cylinder center and the doublet, i.e. at a dimensionless distance of $1/\ell$ from the cylinder center with an orientation *antiparallel* to that of the doublet. These doublets form the *second generation.*

(3) We repeat the image generation process of item 2 for the second generation doublets creating a third generation of doublets and so on, checking at each iteration if the BC of zero velocity normal to all cylinder surfaces* (impenetrability) is satisfied to within a prescribed tolerance (typically 10^{-5}). At this point we have a distribution of doublets which when taken together with the uniform flow at upstream infinity satisfy Laplace's equation for the velocity potential and the associated BCs. For the irrotational flow considered here this distribution of doublets suffices to determine uniquely the flow field.

The MOI is computationally very simple and typical programs have relatively few lines of code. The above mentioned loop is used repeatedly to calculate new generations of doublets by applying the image relations to the previous generations of doublets. One major advantage of the MOI over other techniques is the ability to calculate the velocity field at any point in the flow and not just at selected grid or node points. In this way interpolation of the flow field during the calculation of particle trajectories is avoided and thus a source of numerical error is eliminated.

The number of doublets generated with the MOI, N_d, depends on N_{cyl} and the number of doublet generations performed. After N generations we find that N_d is given by:

$$N_d = N_{cyl} \cdot \sum_{k=1}^{N} (N_{cyl}-1)^{k-1}. \tag{9}$$

As may be seen from Fig. 1, the number of doublets grows exponentially with the number of generations and the number of cylinders in the array. The number of generations required to obtain an accurate result depends on the array geometry. For close spacings ($S<2.5$) and/or many collectors, the CPU memory (and time) requirements of the MOI increase substantially. For example, five generations for an array containing 15 cylinders are sufficient to approach the memory limit of the workstation used in these calculations. We have therefore explored several series acceleration techniques using the results of intermediate steps to improve convergence. Of these techniques, Shank's transformation (see, e.g., Van Dyke, 1974) was found to be well suited for our calculations. For example, convergence to the fifth decimal digit could be obtained for cylinder assemblies containing up to five cylinders after five doublet generations and repeated application of Shank's transformation.

* We found that monitoring the convergence of the central cylinder's stagnation point velocity and its gradient was a conservative criterion for satisfaction of the BCs on all cylinder surfaces. in the 'column' of cylinders.

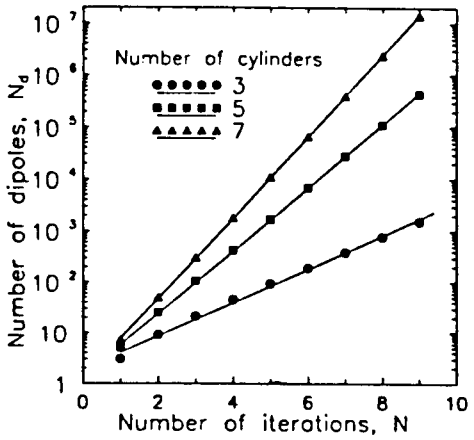

Fig. 1. Dependence of number of doublets on number of generations and number of collectors in the array(column)

This is equivalent to the results obtained after 10 generations without acceleration. Based on these results Shank's transformation was permanently incorporated in our code for extrapolation to the limit of infinite number of generations:

$$S_n' = S_{n+1} - \frac{(S_{n+1} - S_n)^2}{S_{n+1} - 2S_n + S_{n-1}}, \tag{10}$$

where S_ns are partial sums of the image series and S_n' is an improved estimate for the $n \to \infty$ limit.

The infinite array problem is equivalent to that of a cylinder placed in a "frictionless duct" with walls parallel to the x-axis, of width equal to the spacing of the infinite array. In this case, an initially placed doublet at the center of the cylinder is reflected across the "duct walls" and the image generation sequence proceeds as in the case of the finite array. We had no problem in converging on the correct solution, that contained the duct walls as streamlines, for $S > 3$. For $S < 3$ however, due to the stronger image interactions the streamlines of the flow field generated with the method described, did not exactly coincide with the duct walls due to fluid "leakage" across them. To correct for this situation we found it convenient to add a few regularly spaced undetermined singularities on the y-axis. The strength of these singularities was determined by requiring no side leakage across the duct walls, at an equal number of equidistant collocation points, placed along the walls, extending to $10R$ from the origin.

From Levin's theorem given in the Appendix, we know that the value of the stagnation point velocity gradient in potential flows plays a crucial role in determining the onset of inertial impaction by imposing the value of $\mathrm{Stk}_{\mathrm{crit}}$, below which no capture occurs. It is then appropriate at this point to examine the influence of N_{cyl} and S on the dimensionless (normalized with U_∞/R) velocity gradient $[\mathrm{d}u/\mathrm{d}x]_{\mathrm{sp}}$. For an isolated cylinder the result is well-known: $[\mathrm{d}u/\mathrm{d}x]_{\mathrm{sp},S=\infty} = 2$.

Figure 2 depicts the influence of the number of cylinders in the array on $[\mathrm{d}u/\mathrm{d}x]_{\mathrm{sp}}$ of the central cylinder for a fixed spacing $S = 4$. The dashed line is the infinite array limit, $[\mathrm{d}u/\mathrm{d}x]_{\mathrm{sp},N_{\mathrm{cyl}}=\infty} = 2.3534$. As expected, increasing the number of cylinders creates larger velocities in the vicinity of the collector due to the smaller area available to the flow and accordingly, larger gradients, since the flow must decelerate locally from a larger value to zero as the stagnation point is reached. Figure 3 shows the effect of S on $[\mathrm{d}u/\mathrm{d}x]_{\mathrm{sp}}$ for the infinite array. This figure also includes experimental results (open symbols) extracted from "blockage factor" measurements of high-Re momentum and heat transfer to a cylinder in a duct given in Žukauskas and Žiugžda (1985). The potential flow model captures correctly the relative trends but lies consistently below the measurements as if the experiments

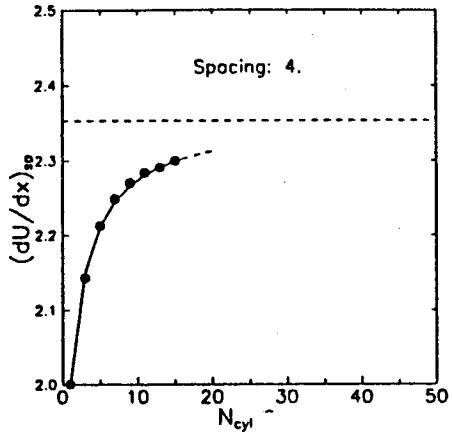

Fig. 2. Dimensionless stagnation point velocity gradient of central cylinder for $S=4$ as a function of the number of cylinders in the array. The dashed line is the infinite array limit.

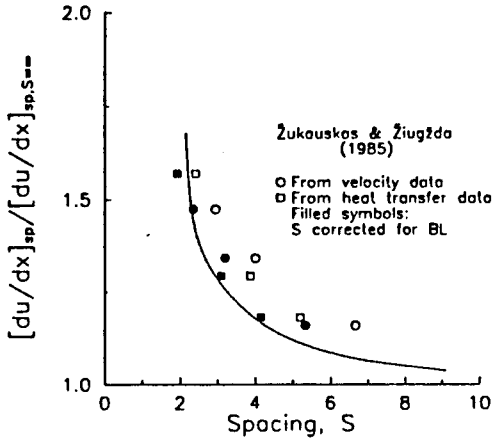

Fig. 3. Dimensionless stagnation point velocity gradient of a cylinder in an infinite array as a function of S. Experimental measurements for a cylinder in a duct, extracted from Žukauskas and Žiugžda (1985).

corresponded to a higher "effective blockage" (smaller spacing) than actual. A possible cause for this might be that the boundary layers (BLs) on the cylinder and on the duct wall increase the "effective blockage" by displacing the adjacent flow, driving thus the stagnation point gradients higher. Indeed, when we correct approximately for such effects by subtracting from S the estimated total thickness of the boundary layers on the cylinder and duct walls (filled symbols in Fig. 3) the agreement between measurements and theory becomes much better.

Our results for $[du/dx]_{sp}$ for the central ("test") cylinder of the array as a function of spacing are shown in Fig. 4. Interestingly enough, $[du/dx]_{sp}$ develops a maximum for S near 3.5 for $N_{cyl}=3$ which increases in magnitude and moves toward smaller S values as N_{cyl} grows. The non-monotonic behavior seen in Fig. 4 is the result of the competition between "flow through" (dominant at large S) and "flow around" (dominant at small S) the arrays containing a finite number of cylinders. This effect is, of course, absent for the infinite arrays, where "flow around" the array cannot occur.

The non-monotonicity in $[du/dx]_{sp}$ for finite arrays, implies that there is an optimum spacing for the capture of particles of a given size near the onset of inertial impaction on the central cylinder, since Stk for this spacing will reach its critical value sooner than for other

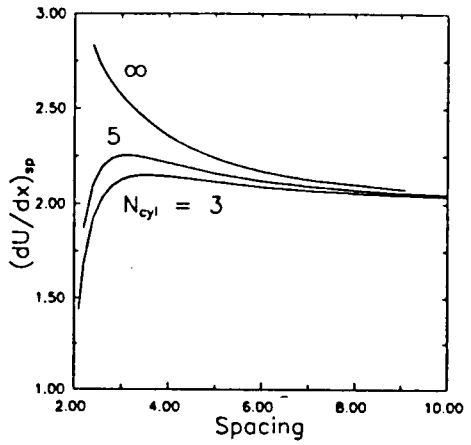

Fig. 4. Stagnation point velocity gradient of central cylinder, dependence on S for various arrays.

spacings (see also section 4). This fact means that if the purpose is to decrease deposition this optimal spacing must be avoided, while if the goal is to maximize collection this spacing should be selected. The graph of Fig. 4 also suggests that is possible to develop a continuously adjustable inertial separation scheme using a cylinder array, the spacing of which could be varied by a mechanical arrangement, effectively changing *on-line* $\mathrm{Stk}_{\mathrm{crit}}$ and consequently the collection characteristics of the array.

3. CAPTURE EFFICIENCY

We employed what might be called a "finite-analytic" technique for computationally efficient integrations of the particle momentum equation, given below, because many trajectory integrations had to be performed:

$$\frac{D\mathbf{u}_p}{Dt}=\frac{\mathbf{u}-\mathbf{u}_p}{\tau}. \tag{11}$$

The essence of the technique is to use a locally-valid, analytic solution for particle motion in a piece-wise fashion, so as to be able to take large time steps in integrating the equation of motion. Our code employs two such solutions, appropriate for:

(1) particle motion in a linear flow field (see also, Fernández de la Mora, 1985); and
(2) particle motion in a constant flow field (see, e.g., Fuchs, 1964).

In equation (11) we use Stokes' drag law for simplicity, since Israel and Rosner (1983) have already shown how to take into account non-linear drag laws in $\mathrm{Stk}_{\mathrm{eff}}$. The particles are injected in equilibrium with the flow at upstream infinity:

$$\mathbf{u}_p\{-\infty, y\}=U_\infty \hat{\mathbf{e}}_x \tag{12}$$

and are advanced to a predetermined distance ($x=-50R$ is an acceptable value in terms of speed of execution and accuracy in the calculation of capture efficiency) using the aforementioned analytic solution for motion in an (approximately) constant flow field. The integration then proceeds using the solution for motion in a piece-wise linear flow field. The capture efficiency is evaluated as usual using a limiting trajectory scheme (see e.g. Fuchs, 1964), computed iteratively with a bisection technique. In the calculations reported here we treat the particles as point masses and neglect the phenomenon of interception, an assumption certainly valid considering the relative sizes of suspended particles and tube collectors occurring in the heat exchanger fouling applications of interest to us ($d_p/2R<10^{-4}$). Inclusion of the interception effect is straightforward (e.g., Fuchs, 1964), but it adds an

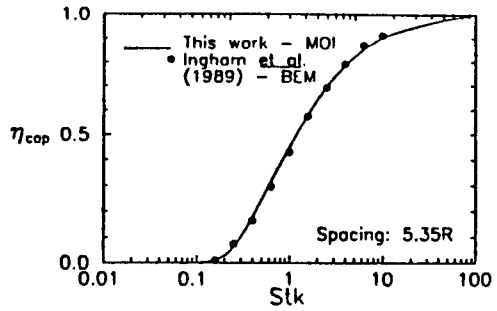

Fig. 5. Comparison of present capture efficiency calculation to the results of Ingham *et al.* (1989) for $S \cong 5.35$.

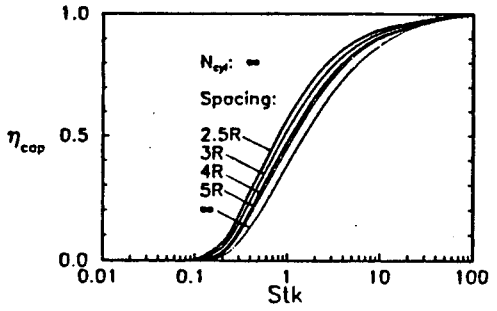

Fig. 6. Capture efficiency of central cylinder in infinite cylinder arrays as a function of Stk at various spacings.

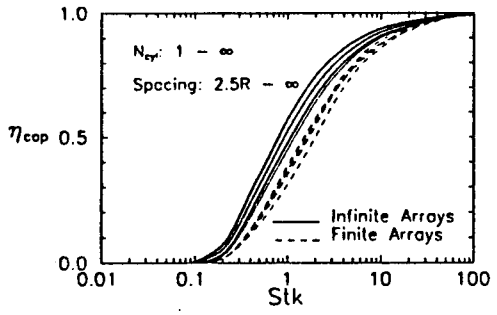

Fig. 7. Capture efficiency of central cylinder in finite and infinite cylinder arrays as a function of Stk at various spacings. Starting from the uppermost solid curve S: 2.5, 3, 4, 5, ∞, 4, 3, 10, 2.5.

additional variable, the interception parameter, $d_p/(2R)$ to the parameter space of the present problem, $\{N_{cyl}, S, \text{Stk}\}$.

In Fig. 5, we compare our $\eta_{cap}(\text{Stk})$ results for an infinite array with $S = 5.35$ to those of Ingham *et al.* (1989), as read from curve B in Fig. 5 of their paper. It can be seen that the agreement is excellent, and justifies the asymptotic approximations that Ingham *et al.* (1989) employed to reduce the computational burden of their flow field calculation [cf. their equations (5)–(12)].

We summarize our results for infinite arrays at various values of S from 2.5 to ∞ in Fig. 6. As expected from the results of Fig. 4, decreasing S makes it easier for particles to impact and consequently the capture efficiency increases. The maximum increases occur for $\text{Stk} \sim \mathcal{O}(1)$ since for $\text{Stk} \to \infty$ the value of η_{cap} must approach 1 irrespective of the spacing of the array. Figure 7 shows the capture efficiency of both finite and infinite arrays. Interesti-

ngly enough, the finite array results for the same spacing are always lower than the infinite array results. Both sets of results follow the "ordering" of the $[du/dx]_{sp}$ curves of Fig. 4.

4. CORRELATIONS

Motivated by Levin's theorem (Appendix) that gives Stk_{crit} in terms of the carrier fluid stagnation point velocity gradient, we define an *effective* Stokes number, Stk_{eff} basing the characteristic flow time on the (dimensional) stagnation point fluid deceleration rate, $[du/dx]_{sp}^{-1}$:

$$Stk_{eff} \equiv \frac{\tau}{2\left[\frac{du}{dx}\right]_{sp}^{-1}}. \tag{13}$$

This definition, in combination with Levin's theorem, maps the critical Stokes number ($=\tau U_\infty/R$) for each array configuration, onto the isolated collector value of 1/8. Based on these considerations we conjecture (see also, Israel and Rosner, 1983) that this definition will also make possible the correlation of the capture characteristics of the different arrays in terms of a single "universal" curve.

The results shown in Fig. 8, provide partial support for this conjecture. The open data points correspond to finite regular arrays and the filled points to infinite arrays. The solid line in Fig. 8 corresponds to the infinite spacing limit (i.e., the isolated collector). In other words, the isolated collector η_{cap} value computed at the prevailing Stk_{eff} can serve as an engineering approximation for the collection efficiency of the "test" cylinder. Comparing Fig. 8 to Fig. 7 note how the present correlation scheme is especially successful in compressing the data in the vicinity of Stk_{crit} on a single curve. Although the spread increases at higher Stk_{eff}-values, the correlation scheme may be sufficient for engineering estimates for all Stk-values since the fractional error between the solid curve and the data is decreasing with increasing Stk_{eff}. A better correlation would have been obtained if we eliminated the open circles which correspond to a closely-packed ($S=2.5$) three cylinder array. This array geometry is closer to that of a ribbon in cross-flow than an isolated cylinder, and the flow field in the vicinity of the test collector is quite different from the other cases. The observed spread at high Stk_{eff} is due to the fact that in this limit, the various array flow fields experienced by the particles, are more dissimilar than the "almost universal" stagnation flow regions experienced by slightly supercritical particles. For completeness, we cite the Israel and Rosner (1983) correlation, for $\eta_{cap}\{Stk_{eff}\}$ (extended here to the case of cylinder arrays) valid for $Stk_{eff} > 0.14$†, although, as mentioned, other acceptable alternat-

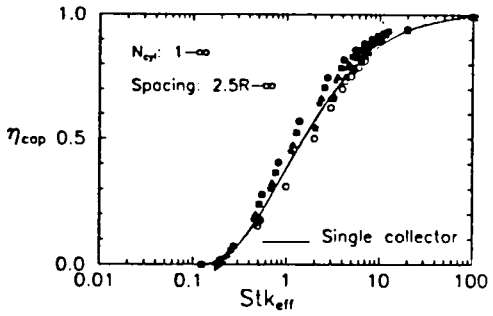

Fig. 8. Correlation of inertial impaction capture efficiency of a central cylinder in finite (open symbols) and infinite (filled symbols) arrays in terms of Stk_{eff}. Circles correspond to $S=2.5$, squares to 3, triangles to 4 and stars to 5. The solid line is the isolated collector curve.

† The behavior of $\eta_{cap}\{Stk_{eff}\}$ for $Stk_{eff} \to Stk_{crit}$ is non-analytic and is discussed in a set of unpublished notes by Prof. J. Fernández de la Mora (1985).

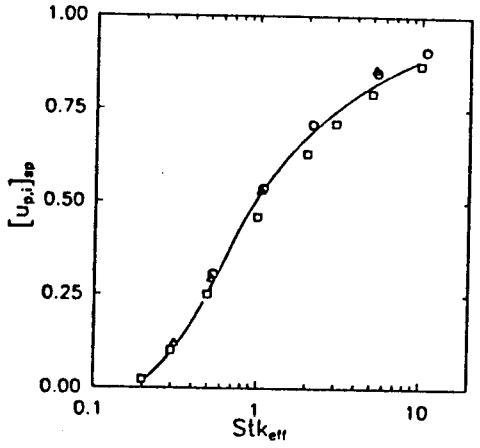

Fig. 9. Correlation of stagnation point impact velocity, $[u_{p,i}]_{sp}$ for the central cylinder, in an array of three collectors, at $S=2.5$ (squares), 4 (circles), ∞ (triangles), in terms of Stk_{eff}.

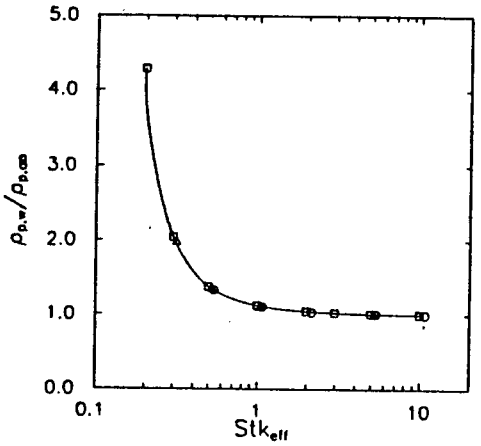

Fig. 10. Correlation of stagnation point particle concentration enrichment $\rho_{p,w}/\rho_{p,\infty}$ for the central cylinder, in an array of three collectors, at $S=2.5$ (squares), 4 (circles), ∞ (triangles), in terms of Stk_{eff}.

ives (Wang, 1986; Wessel and Righi, 1988) also exist:

$$\eta_{cap}(Stk_{eff}) \approx [1 + 1.25(Stk_{eff} - \tfrac{1}{8})^{-1} - 1.4 \times 10^{-2}(Stk_{eff} - \tfrac{1}{8})^{-2} + 0.508 \times 10^{-4}(Stk_{eff} - \tfrac{1}{8})^{-3}]^{-1}. \quad (14)$$

Correlation of the data in terms of Stk_{eff} seems to be possible for other quantities of interest as well (at least for an array of three collectors tested so far), such as impact velocities at the stagnation point (Fig. 9), concentration enrichment factors (Fig. 10), etc., which will be addressed in more detail in the future.

5. CONCLUDING REMARKS

Inertial impaction calculations for linear, regularly spaced, circular cylinder arrays reveal that the principal effect of multiple target proximity is to change the local gas deceleration rates of the carrier fluid, thereby shifting Stk_{crit}. Thus, our numerical results for particle capture on the central cylinder in arrays containing from three to an infinite number of flanking cylinders, are fairly well-correlated using the relevant, *effective* Stokes number, Stk_{eff}, i.e. basing the "characteristic flow time" on the actual (not on the isolated-target)

gas deceleration rate in the vicinity of the stagnation point. Overall, it now appears possible to make engineering estimates for the capture efficiency of fluid-dynamically interacting cylinders in inviscid, cross-flow from a knowledge of the stagnation point gradient, given in Fig. 4 as a function of number of cylinders and spacing, and the well-known correlations for a single cylinder (Israel and Rosner, 1983; Wang, 1986; Wessel and Righi, 1989). Work in progress in this area is focusing on extending the correlation approach to angular distributions of quantities of interest, examining other cylinder arrangements (e.g. staggered arrays) as well as studying asymmetric deposition patterns on the side cylinders.

It would also be of interest to compute (using the inviscid velocity distributions on the surface of the collector) the fluid mechanics of the boundary layer (BL) developing along the cylinder surface, to estimate collector proximity effects on BL mass, momentum and heat transfer rates to our representative cylinder in the array. We note however, that self-similar BL solutions based on the inviscid stagnation point velocity gradient (Fig. 4), are often acceptable engineering approximations to the flow up to *ca* 20° from the stagnation point of the bluff collector (Schlichting, 1955), where a significant part of deposition also occurs in practice (Rosner, 1986). It is straightforward then to estimate deposition rates for this geometry under the *simultaneous* action of inertial ($Stk < Stk_{crit}$) and thermophoretic/diffusive effects applying correlations and boundary layer deposition theory for curved walls (Konstandopoulos and Rosner, 1990; Konstandopoulos, 1991).

Furthermore, while we have deliberately assumed that particles arriving at the surface do not rebound upon impact, the present results can easily be corrected for effects of incomplete particle capture using analytic expressions for the sticking coefficient of particles impacting clean collectors (Konstandopoulos, 1991; Wang and John, 1988). Along these lines, the stage is now also set for extensions of the calculations performed here to account for hydrodynamic interference effects due to thick deposit growth on the collector (*cf.* Rosner and Günes, 1993). An attractive route would be to explore, for example, conformal mapping techniques in order to "deform" the non-circular collector cross-section, resulting from deposit accumulation on the cylinder, back to a circular shape. In addition, such calculations can now incorporate sticking coefficients of particles impacting on deposits, extracted from discrete-particle simulations of deposit growth (Konstandopoulos, 1991; Konstandopoulos and Tassopoulos, 1990).

Acknowledgements—We are indebted to Profs J. Fernández de la Mora (Yale, Department of Mechanical Engineering), P. Garcia-Ybarra and J. Castillo (Department of Fundamental Physics, UNED, Spain) for helpful discussions and comments. This work has been supported in part by the U.S. Department of Energy-Pittsburgh Energy Technology Center, under Grant No. DE-FG-90-PC 90099 and the Yale HTCRE Laboratory Industrial Affiliates (Union Carbide, E. I. DuPont de Nemours and Co., General Electric, Shell and SCM-Chemicals).

REFERENCES

Choudhary, K. R. and Gentry, J. W. (1977) A model for particle collection with potential flow between two parallel cylinders. *Canadian J. Chem. Eng.* **55**, 403–407.

Davies, C. N. (1966) *Aerosol Science*. Academic Press, New York.

Fan, J., Zhou, D., Jin, J. and Cen, K. (1991) Numerical calculation of tube bundle erosion by turbulent particle-laden gas flows. *Chem. Eng. Comm.* **104**, 209–225.

Fernández de la Mora, J. (1985) Inertial effects on linear and locally linear flows. *Aerosol Sci. Technol.* **4**, 339–349.

Fletcher, C. A. J. (1988) *Computational Techniques for Fluid Dynamics*. Springer, New York.

Fuchs, N. A. (1964) *The Mechanics of Aerosols*. Pergamon, New York. Also available as Dover Publications (N.Y.) Paperback. No. 0-486-66055-9 (1989).

Friedlander, S. K. (1977) *Smoke Dust and Haze: Fundamentals of Aerosol Behavior*. Wiley, New York.

Ilias, S. and Douglas, P. L. (1989) Inertial impaction of aerosol particles on cylinders at intermediate and high Reynolds numbers. *Chem. Eng. Sci.* **44**, 81–99.

Ingham, D. B., Hildyard, M. L. and Heggs, P. J. (1989) The particle collection efficiency of a cascade of cylinders. *Canadian J. Chem. Eng.* **67**, 545–553.

Ingham, D. B., Hildyard, L. T. and Hildyard, M. L. (1990) On the critical Stokes number for particle transport in potential and viscous flows near bluff bodies. *J. Aerosol Sci.* **21**, 935–946.

Israel, R. and Rosner, D. E. (1983) Use of a generalized Stokes number to determine the aerodynamic capture efficiency of non-stokesian particles from a compressible gas flow. *Aerosol Sci. Technol. (AAAR)* **9**, 29–60.

Konstandopoulos, A. G. (1991) Effects of particle inertia on aerosol transport and deposit growth dynamics. PhD Dissertation, Yale University, New Haven, Connecticut.

IJHMT (in press 1993)

Konstandopoulos, A. G. and Rosner, D. E. (1990) Inertial effects on thermophoretic transport of small particles to walls with streamwise curvature. *AAAR 1990 Annual Meeting*, paper 7C.6, 18–22 June, Philadelphia, PA.

Konstandopoulos, A. G. and Tassopoulos, M. (1990) Simulation of particle impaction: sticking probability and microstructure evolution in the 'frozen' deposit limit. *AAAR 1990 Annual Meeting*, paper 6E.6, 18–22 June, Philadelphia, PA.

Lamb, H. (1932) *Hydrodynamics*, 6th edition. Cambridge University Press, Cambridge. Also available as Dover Paperback. 5256 (1945)

Levin, L. M. (1961) *Issledovaniya po Fizike Grubodispersnykh Aerozoley* (Investigations in the Physics of Coarse Dispersed Aerosols). *Izdatel'stvo Akademii Nauk SSSR*, Institut Prikladnoy Geofisiki, Moscow. English translation as Foreign Technology Division Document No. FTD-HT-23-1593-67.

May, K. R. and Clifford (1967) The impaction of aerosol particles on cylinders, spheres, ribbons and disks. *Ann. Occup. Hyg.* **10**, 83–95.

McLaughlin, C., McComber, P. and Gakwaya, A. (1986) Numerical calculation of particle collection by a row of cylinders in a viscous fluid. *Canadian J. Chem. Eng.* **64**, 205–210.

Michael, D. H. and Norey, P. W. (1970) Slow motion of a sphere in a two-phase medium. *Canadian J. Phys.* **48**, 1607–1616.

Milne-Thomson, L. M. (1955) *Theoretical Hydrodynamics*, 3rd edition. Macmillan, New York.

Rosner, D. E. (1986) *Transport Processes in Chemically Reacting Flow Systems*. third printing (1990), Butterworth-Heinemann, Stoneham, MA.

Rosner, D. E. and Günes, D. (1993) Theory of deposit shape evolution for heat exchanger surfaces exposed to the flow of fly-ash containing combustion products, based on the 1987 Yale-HTCRE Lab Internal Report (to be submitted).

Schlichting, H. (1955) *Boundary Layer Theory*. McGraw-Hill, New York.

Schuh, M. J., Schuler, C. A. and Humphrey, J. A. C. (1989) Numerical calculation of particle-laden gas flows past tubes. *AIChE J.* **35**, 466–480.

Tien, C. (1989) *Granular Filtration of Aerosols and Hydrosols*. Butterworths, Stoneham, MA.

Tsiang, R. C., Wang, C. S. and Tien, C. (1982) Dynamics of particle deposition on model fibre filters. *Chem. Eng. Sci.* **37**, 1661–1673.

Van Dyke, M. (1974) Analysis and improvement of perturbation series. *Q. J. Mech. Appl. Math.* XXVII, 421–450.

Wang, H. C. (1986) Theoretical adhesion efficiency for particles impacting a cylinder at high Reynolds number. *J. Aerosol Sci.* **17**, 827–837.

Wang, H. C. and John, W. (1988) Dynamic adhesion of particles impacting a cylinder. In *Particles on Surfaces* (Edited by K. L. Mittal), pp. 211–224. Plenum Press, New York.

Wessel, R. A. and Righi, J. (1988) Generalized correlations for inertial impaction of particles on a circular cylinder. *Aerosol Sci. Technol.* **9**, 29–60.

Žukauskas, A. and Žiugžda, J. (1985) *Heat Transfer on a Cylinder in Cross Flow*. Hemisphere, Washington.

APPENDIX: ON THE CRITICAL STOKES NUMBER

It has been known for quite some time that, under certain conditions, there exists a finite, critical Stokes number, Stk_{crit}, for inertial impaction from flows past bluff bodies. For $Stk < Stk_{crit}$ no particle trajectory which is in equilibrium with the flow at infinity reaches the surface with finite velocity, in the absence of other transport mechanisms. Taylor [1940] obtained the value of Stk_{crit} for impaction from inviscid, stagnation-point flow, making certain assumptions about the initial conditions of the particles, while general conditions for, and proof of, the existence of Stk_{crit} for inviscid flows past bluff bodies, were summarized in an important yet not widely known (in the Western literature) monograph by Levin (1961). We will term this proof Levin's theorem, stated below (paraphrasing excerpts from Levin (1961)) as:

> LEVIN'S THEOREM: For flows past axially or n-th order ($n \geq 2$) rotationally symmetrical bodies of characteristic dimension L, which are parallel to the body's axis of symmetry at infinity (with velocity U_∞), and the streamlines of which terminate at the upstream stagnation point as straight lines with slope α, there exists a critical Stokes number, $Stk_{crit} \equiv \tau U_\infty / L = 1/(4\alpha)$, for a broad range of initial conditions,* below which no particle reaches the body.

More recently, in an article published in this *Journal*, Ingham *et al.* (1990) have also given a detailed proof of the essence of Levin's theorem for potential flows and suggested that Stk_{crit} for viscous flows is zero. They reached this conclusion by examining particle trajectories in the quadratic flow $u = bx^2$ obtained as the leading term of the Taylor expansion† of the normal component of the fluid velocity, u in the distance x from a boundary surface. However, Levin (1961) has proven the *existence of* $Stk_{crit} > 0$ *for viscous flows* as well, given appropriate initial conditions. Levin implicitly recognized that in this case the onset of inertial impaction is governed by phenomena occurring in a region where the quadratic flow is a poor approximation to the flow field, but he nevertheless suggested a scaling relation: $Stk_{crit} = \text{const.}\ b^{-1/2}$, and evaluated the constant by comparison to numerical estimates of Stk_{crit} of viscous flows. Although $Stk_{crit} > 0$ has been reported based on numerical studies for some viscous flow cases (Fuchs, 1964; Levin, 1961), it is also possible to compute Stk_{crit} semi-analytically following the approach of Michael and Norey (1970). These authors treated carefully the singularity of the particle momentum equation at the stagnation point and calculated Stk_{crit} for inertial impaction from creeping flow past a sphere to be 1.21194. Langmuir [1948] had obtained numerically for that case $Stk_{crit} \approx 1.214$.

---

* Discussed by Levin (1961); see also, Fernández de la Mora (1980, 1985) and Ingham *et al.* (1990).

† This quadratic dependence is a consequence of the no-slip condition of the ~~streamwise~~ tangential component of the velocity and incompressibility.

Deposition of particles from potential flows

In closing we recall that, as Fernández de la Mora (1985) has shown, for arbitrary linear and locally linear flows characterized by a deceleration time scale ω^{-1}, the particle motion becomes critically damped by the host-flow when the product ωt becomes equal to $1/[4\max(\lambda_i)]$ where λ_i stands for any of the eigenvalues of the velocity gradient tensor (rendered dimensionless with ω). Whether the $\mathrm{Stk}_* \equiv 1/[4\max(\lambda_i)]$ thus determined coincides with Stk_{crit} for inertial impaction, depends on the nature of the flow field. The two numbers coincide for potential flows where the maximum velocity gradient occurs on the boundary of the body.

For viscous flows however, Stk_{crit} can be significantly higher than Stk_* due to the fact that the maximum velocity gradient occurs away from the collector wall and the particle motion has the chance to become overdamped again, inside the almost stagnant viscous region adjacent to the wall. For example, in the case of creeping flow past a sphere, the particle motion becomes first underdamped for $\mathrm{Stk}_* > 2/3$ at a distance $(\sqrt{2}-1)R$ from the sphere surface along the stagnation line where the maximum velocity gradient occurs, yet Stk_{crit} for this flow as we saw above is 1.21194. Similarly, for a cylinder in Oseen flow, underdamping at first occurs when $\mathrm{Stk}_* > 0.6495(2.002 - \ln \mathrm{Re})^{-1}$ at a distance $(\sqrt{3}-1)R$ from the surface along the stagnation line. Stk_{crit} for this case is reported to be 4.3 ± 0.1 for $\mathrm{Re} = 0.1$ (Fuchs, 1964).

See, also:

Aerosol Science and Technology 2:45-51 (1983)

Use of a Generalized Stokes Number to Determine the Aerodynamic Capture Efficiency of Non-Stokesian Particles from a Compressible Gas Flow

R. Israel and D. E. Rosner

High Temperature Chemical Reaction Engineering Laboratory, Chemical Engineering Department, Yale University, New Haven, CT 06520

The aerodynamic capture efficiency of small but non-diffusing particles suspended in a high-speed stream flowing past a target is known to be influenced by parameters governing (a) small particle *inertia*, (b) departures from the Stokes drag law (associated with local particle Reynolds numbers greater than unity), and (c) carrier fluid compressibility (at nonnegligible free-stream Mach numbers). By defining an *effective Stokes number* in terms of the actual (prevailing) particle stopping distance, local fluid viscosity, and inviscid fluid velocity gradient at the target nose, we show that these effects are well correlated in terms of a "standard" (cylindrical collector, Stokes drag, incompressible flow, $\mathrm{Re}^{1/2} \gg 1$) capture efficiency curve. We are thus led to a correlation that (a) simplifies aerosol capture calculations in the parameter range already included in previous numerical solutions, (b) allows rational engineering predictions of deposition in situations not previously specifically calculated, (c) should facilitate the presentation of performance data for gas cleaning equipment and aerosol instruments.

HIGH TEMPERATURE CHEMICAL REACTION
ENGINEERING LABORATORY
YALE UNIVERSITY
BOX 2159, YALE STATION
NEW HAVEN, CONNECTICUT 06520 U.S.A.